THE GEOLOGICAL SOCIETY OF AMERICA®

Ediacaran coupling of climate and biosphere dynamics

Thomas W. Wong Hearing[1,†], Benjamin H. Tindal[2], Thomas M. Vandyk[1], Lin Na[1,3], Alexandre Pohl[4], Alexander G. Liu[5], Thomas H.P. Harvey[1], and Mark Williams[1]

[1]*Centre for Palaeobiology and Biosphere Evolution, School of Geography, Geology and the Environment, University of Leicester, Leicester LE1 7RH, UK*

[2]*Chief Scientist's Directorate, Natural England, 8 City Walk, Leeds LS11 9AT, UK*

[3]*State Key Laboratory of Palaeobiology and Stratigraphy, Nanjing Institute of Geology and Palaeontology, Chinese Academy of Sciences, Beijing East Road 39, 210008 Nanjing, China*

[4]*Université Bourgogne Europe, Centre National de la Recherche Scientifique (CNRS), Biogéosciences UMR 6282, 21000 Dijon, France*

[5]*Department of Earth Sciences, University of Cambridge, Downing Street, Cambridge CB2 3EQ, UK*

ABSTRACT

Climate change is demonstrably linked to radiations, extinctions, and turnovers in the biosphere throughout the Phanerozoic (538.8 Ma to present). Here, we suggest this connection existed as early as the late Ediacaran (ca. 579–538.8 Ma), the first interval in Earth's history to host complex macroscopic organisms, including early animals. We systematically evaluated the dating, correlation, and likely glaciogenicity of candidate Ediacaran glaciogenic deposits to produce a first-order climatic framework for the middle to late Ediacaran. In contrast to previous studies, we accounted for uncertainties in chronostratigraphy, correlation, and depositional interpretation of candidate glaciogenic deposits and thereby reduced the error envelopes that supported previous interpretations of either one long (>20 m.y.) or up to four short (1–5 m.y.) icehouse intervals. Despite large uncertainties regarding the precise ages of many late Ediacaran deposits, we show that the most parsimonious explanation of available data identifies two intervals of icehouse climate (mid-Ediacaran, ca. 593–579 Ma, and late Ediacaran, ca. 565 Ma to ca. 550 Ma) that alternated with greenhouse climates (late Ediacaran, ca. 579–565 Ma, and terminal Ediacaran, ca. 550 Ma to Cambrian). Sedimentological data suggest that both icehouse intervals were characterized by geographically restricted glaciations with repeated expansion and contraction of ice sheets. The changes in climate state we propose were contemporaneous with turnovers in the late Ediacaran biosphere. Further data collection is required to test our climate framework, but current evidence supports a Phanerozoic-style coupling of global climate and biosphere during the early stages of animal evolution.

INTRODUCTION

Changes in Earth's climate and biosphere are closely linked throughout the Phanerozoic Eon (the past ~539 m.y.). Transitions between globally cooler and warmer conditions are implicated in extinctions, diversifications, and biotic turnovers in the Phanerozoic fossil record (e.g., Erwin, 2009; Bond and Grasby, 2017; Fenton et al., 2023; Woodhouse et al., 2023). However, it is unclear whether such relationships existed in Earth's earliest known metazoan biosphere, that of the late Ediacaran Period (ca. 580–538.8 Ma). The Ediacaran Period followed the Cryogenian Period, which was supposedly characterized by extreme and long-lasting "snowball" climate conditions (e.g., Hoffman et al., 2017), and preceded the prolonged greenhouse climate of the Cambrian Period (Scotese et al., 2021; Wong Hearing et al., 2021). The Ediacaran Period can therefore be viewed as a transitional interval in Earth's climate history, coincident with the early diversification of animals (Butterfield, 2009; Wood et al., 2019; Xiao and Narbonne, 2020).

Evidence for glaciogenic sedimentary deposits of broadly mid- to late Ediacaran age has been widely recognized in the rock record (e.g., Brückner and Anderson, 1971; Anderson, 1972; Hambrey and Harland, 1981b; Chumakov, 2007, 2009). Candidate Ediacaran glacial deposits have been variously considered to represent either several very short glaciations (e.g., Pu et al., 2016; Retallack, 2022; Linnemann et al., 2022; Niu et al., 2024) or one continuous 20–40 m.y. icehouse interval with a shifting locus (e.g., Wang et al., 2023a, 2023b). These studies all propose testable hypotheses of a first-order climatic framework for the mid- to late Ediacaran Period. Testing these hypotheses requires a systematic consideration of both the depositional ages and genesis of the rocks on which they rest. However, recent compilations of candidate Ediacaran glacial units have applied inconsistent criteria to assemble only partially overlapping subsets of deposits (Fig. 1) within different correlation frameworks (Table 1; Fig. S1 in the Supplemental Material;[1] Youbi et al., 2020; Retallack, 2022; Wang et al., 2023a, 2023b; Niu et al., 2024). The resulting uncertainty about which deposits are glacial and how they should be correlated has hindered assessments of Earth's climate evolution through this critical interval in biosphere evolution. It remains unclear, for example, whether the largest carbon cycle perturbation in the geological record, the Shuram excursion with $\delta^{13}C$ values as low as −12‰, occurred when Earth was in a greenhouse (Shields et al., 2019; Bergmann et al., 2022) or an icehouse (Wang et al., 2023a, 2023b) climate state.

Thomas Wong Hearing https://orcid.org/0000-0002-6770-6433
[†]twonghearing@gmail.com

[1]Supplemental Material. Text S1: Additional text and figures supporting the main text (Table S7; Figures S1–S6). Data S1: Excel file of candidate Ediacaran glaciogenic deposits (Tables S1–S3). Data S2: Excel file of Ediacaran paleontological data occurrences (Tables S4–S6, S8, and S9). The R code required to reproduce all figures and analysis can be found at https://github.com/twwh01/Ediacaran_climate_framework. Please visit https://doi.org/10.1130/GSAB.S.33170042 to access the supplemental material; contact editing@geosociety.org with any questions.

GSA Bulletin;
Published online 17 August 2026
https://doi.org/10.1130/B39047.1.

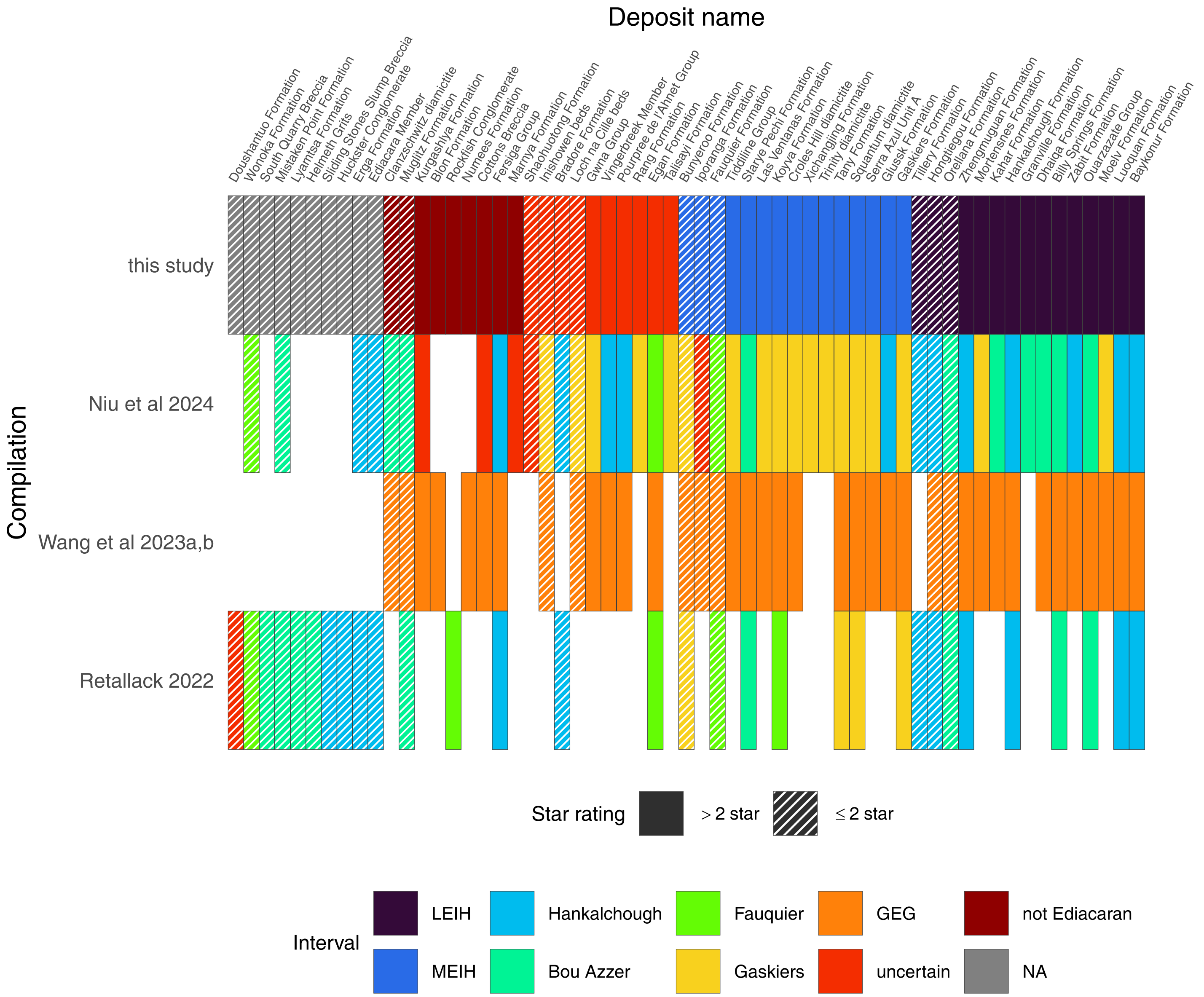

Figure 1. Comparison of the candidate Ediacaran glaciogenic deposits included in our study and in recent compilations (Retallack, 2022; Wang et al., 2023a, 2023b; Niu et al., 2024). Colors indicate the glaciation or interval to which the deposit was assigned by each study. Deposits rated greater than two stars are in solid colors; deposits rated two stars or less are marked by diagonal stripes. LEIH—late Ediacaran icehouse; MEIH—mid-Ediacaran icehouse; GEG—Great Ediacaran glaciation; NA—deposits removed from consideration as candidate glaciogenic units (see the Supplemental Material [text footnote 1]).

TABLE 1. COMPARISON OF PUBLISHED LITERATURE COMPILATIONS AND CORRELATIONS OF CANDIDATE EDIACARAN GLACIAL DEPOSITS

Compilation	Unique deposits	Gaskiers*	Fauquier†	Bou Azzer§	Hankalchough#	GEG**	Other/uncertain
Retallack (2022)	31	4	5	9	12	0	0
Wang et al. (2023a, 2023b)	39	0	0	0	0	39	0
Niu et al. (2024)	50	18	3	10	14	0	5

Note: Each row indicates the total number of Ediacaran glacial deposits identified by the compilation cited, as well as their proposed association with any named glaciation. For reference, and not shown here for legibility: Tindal (2023) identified 224 potentially glaciogenic deposits having radiometric age constraints compatible with Ediacaran deposition, although poor age constraints mean many of these are likely Cryogenian in age; Youbi et al. (2020) identified 25 candidate glaciogenic deposits of Ediacaran age grouped into 12 predominantly local or regional glaciations and concluded that most were plausibly correlated with a ca. 580 Ma Gaskiers glaciation. See also Figure 1 and Supplemental Data S1 (see text footnote 1).

*Gaskiers glaciation: 581–579 Ma (Retallack, 2022; Niu et al., 2024).

†Fauquier glaciation: 572–570 Ma (Retallack, 2022) or 571 Ma (Niu et al., 2024).

§Bou Azzer: 566–564 Ma (Retallack, 2022) or 565–560 Ma (Niu et al., 2024).

#Hankalchough: 555–549 Ma (Retallack, 2022) or 563–551 Ma (Niu et al., 2024).

**GEG—Great Ediacaran glaciation; 580–560 Ma or 594–546 Ma (Wang et al., 2023a, 2023b).

Here, we build on recent advances in stratigraphic correlation (e.g., Rooney et al., 2020; Yang et al., 2021; Busch et al., 2023; Bowyer et al., 2023, 2024) and paleobiology (e.g., Boag et al., 2016, 2024; Muscente et al., 2019; Boddy et al., 2021; Surprenant and Droser, 2024; Bowyer et al., 2024) to interrogate the coevolution of physical and biological components of the Earth system through the Ediacaran Period. Specifically, we combine sedimentological and paleobiological data in a refined chronostratigraphic framework to evaluate the hypothesis that there is a temporal link between global climate state and biodiversity dynamics (faunal turnovers) in the late Ediacaran geological record.

Extrapolating from the Phanerozoic Earth system, we would expect to see in the fossil record a biosphere response to changing climate via changes in standing diversity and/or taxonomic composition (e.g., Erwin, 2009; Woodhouse et al., 2023). The absence of this pattern in the Ediacaran (the null hypothesis) would indicate (1) that geological and collection biases currently obscure our ability to read the Ediacaran geological record, (2) that our data have insufficient age controls for accurate correlation, and/or (3) that the Ediacaran biosphere had a fundamentally different relationship to the climate system than the Phanerozoic biosphere. Understanding past temporal relationships between the biosphere and climate system is essential for evaluating hypotheses of how animal evolution affected Earth's climate evolution and vice versa.

MATERIALS AND METHODS

Climate State

The presence of ice sheets and their size modulate Earth's climate system both qualitatively and quantitatively (e.g., Kidder and Worsley, 2010; Summerhayes, 2020; Westerhold et al., 2020; Judd et al., 2024), as has long been recognized (Fischer, 1981, 1982; Frakes et al., 1992, chapter 1). The presence of ice sheets may be the most reliable indicator of climate state in the geological record (Macdonald et al., 2019; Merdith et al., 2025). Here, we follow definitions of icehouse climate states as times when there were persistent low-altitude ice sheets on Earth, and greenhouse climate states as times when there were no persistent low-altitude ice sheets (e.g., Frakes et al., 1992; Kidder and Worsley, 2010; Pagani et al., 2014; Summerhayes, 2020). We also note that the presence of sea ice alone is insufficient evidence of icehouse conditions. The currently available Ediacaran climate data mean that more precise subdivisions of climate state (e.g., Westerhold et al., 2020; Judd et al., 2024) are not yet appropriate for this interval.

Ediacaran Glacial Deposits

Uniquely, we performed a systematic assessment of both the dating and sedimentological evidence for candidate mid- to late Ediacaran glaciogenic deposits. Although most recent workers have considered the dating evidence for candidate Ediacaran glaciogenic deposits, they have not systematically considered the sedimentological evidence that each deposit was actually formed by ice-related processes, i.e., the likely glaciogenicity (Table 1; Fig. 1). Here, we explicitly and systematically considered the sedimentological evidence for each candidate Ediacaran glaciogenic deposit following the star rating system of Tindal (2023). This rating system is outlined below, summarized in Tables 2 and 3, and described in detail in Tindal's Ph.D. thesis (Tindal, 2023, chapter 2, tables 2.1–2.11).

Our dataset (Supplemental Data S1) is derived from the compilations of Youbi et al. (2020), Retallack (2022), Tindal (2023), Wang et al. (2023a, 2023b), and Niu et al. (2024), with additional data drawn from references cited in those studies, notably Hambrey and Harland (1981b) and Arnaud et al. (2011), as well as more recent publications. All deposits included in the compilations of Youbi et al. (2020), Retallack (2022), Wang et al. (2023a, 2023b), and Niu et al. (2024) were considered here. Deposits not included in these compilations but that were included in Tindal's (2023) appendix 2 were considered where they were rated greater than one star (see "Assessing Glaciogenicity" section) and were plausibly of Ediacaran age (i.e., with an Ediacaran maximum age or mid-Ediacaran to Cambrian minimum age; see the Supplemental Material). After this screening process, many of the remaining deposits from Tindal (2023) are still more likely of Cryogenian than Ediacaran age, based on nonradiometric constraints.

Determining Depositional Age

There is substantial circularity in the dating and correlation of Neoproterozoic putative glaciogenic deposits (Tindal, 2023), which is partly responsible for the discrepancies between previous compilations (Tables 1 and 4; Fig. 1). Putative Neoproterozoic glaciogenic deposits tend to be correlated together on lithostratigraphic grounds ("glaciostratigraphy;" Tindal, 2023). Independent age constraints are therefore crucial for testing potential patterns and quantifying temporal uncertainty in global paleoclimate data.

Literature searches were performed to make rigorous assessments of depositional age for each candidate glaciogenic deposit. Where available, radiometric age constraints were preferred. Radiometric dates were included only if they possessed a well-documented stratigraphic relationship with a candidate glaciogenic deposit. Chemostratigraphic evidence was considered where there is good evidence for regional and global chemostratigraphic correlation. Biostratigraphic age constraints are a valuable but uncertain independent dating method for candidate glaciogenic deposits. In particular, biostratigraphy was useful where Cambrian or Ediacaran fossils are found overlying a diamictite deposit. For example, in northern China, Arabia, and the Baltic region, where the strata overlying diamictite units contain fossils like *Shaanxilithes* that are known to be restricted to the terminal Ediacaran (ca. 550–538.8 Ma; Vickers-Rich et al., 2012; Wang et al., 2021a; Agić et al., 2024). Where we used late Ediacaran macrofossils to provide an age constraint, we assumed that these taxa could extend up to the Ediacaran-Cambrian boundary, and we therefore applied a numerical age constraint of 538.8 Ma following the current International Commission on Stratigraphy chronostratigraphic chart (v2024-12; Cohen et al., 2013; Linnemann et al., 2019), though it is likely that the true age constraint is older than this.

Assessing Glaciogenicity

Putative glaciogenic deposits readily enter the academic literature but are very difficult to excise from it if originally misinterpreted, as shown by the number of low-scoring deposits and the variable range of deposits included in or excluded from previous Ediacaran compilations (Tables 1 and 4; Fig. 1; Tindal, 2023). Neoproterozoic diamictite deposits are frequently interpreted as glaciogenic even when the sedimentology and geotectonic context make a nonglacial origin more parsimonious (e.g., Kennedy et al., 2019; Kennedy and Eyles, 2021; Molén, 2023; Palacios, 2024; Kühnemann et al., 2025; Meinhold et al., 2025). To mitigate for this, we followed the glaciogenicity assessments of Tindal (2023), who devised a semiquantitative five-star rating scheme to assess the strength of evidence for glaciogenicity of deposits and applied it consistently across the pre-Pleistocene glacial record (Tindal, 2023, chapter 2, tables 2.1–2.11).

Tindal's (2023) scheme weights individual lines of sedimentological and geomorphological evidence alongside consideration of the depositional and tectonic context on a zero to five geometric progression scale with common ratio of 2, summarized in Table 2. A rating of five indicates unequivocal evidence for glaciation, and a rating of one means that a broad range of ice-free depositional processes could have been responsible for producing the assembled characteristics (Table 3; Tindal, 2023). The overall star rating for each deposit is the weighted sum of all individual depositional characteristics, such that two lines of evidence at one level equate to one line of evidence at

TABLE 2. SUMMARY OF THE SEDIMENTARY AND GEOMORPHOLOGICAL EVIDENCE USED IN THE TINDAL (2023) STAR RATING SCHEME

Evidence category*	Star rating				
	★★★★★	★★★★	★★★	★★	★
Dropstones[†,§]	—	—	Dropstones in an environment described as flat, distal, or otherwise away from slopes	Dropstones (downslope reworked deposits neither reported nor confirmed absent)	Lonestones or dropstones that are confined to downslope reworked deposits
Clast shape	—	—	—	Elongate or fragile clasts	Clasts from four of Powers' (1953) roundness categories.
Clast surfaces	—	—	Striated clasts	—	Faceted clasts
Erratics and lithologies[#]	—	—	Clasts from four lithological groups, or nonabraded clasts of a distinctive lithology that must have travelled >100 km	Clasts from three lithological groups	Clasts from two lithological groups
Surface striation	Extensive striated surfaces with crescentic gouges, chattermarks and S-forms.	Extensive surfaces with striae and some but not all of the features listed for a five-star deposit.	Extensive surfaces with striae and/or small surfaces with features listed above	Large smooth surfaces and/or small surfaces with striae	Small smooth surfaces
Geomorphological forms	—	—	U-shaped valleys or branching valley networks	Roche moutonneé-like paleotopography, moraine-like ridges	—
Glaciotectonism	—	Extensive surfaces of parallel grooves showing multiple phases of scraping	>10-m-scale cylindrical folding of beds with undeformed underlying beds	Cylindrical folding of beds with undeformed underlying beds	Deformed beds with undeformed underlying beds
Soft sediment ploughing (keel drag)	—	—	Extensive surfaces of parallel grooves	Small surfaces of parallel grooves	Deformed beds
Frost polygons	—	Extensive areas of large polygons with infilled wedges deeper than 20 cm	Extensive areas of large polygons of wedges infilled with coarse material	Large polygonal cracks	Infilled wedges deeper than 20 cm
Cryoturbation	—	—	Extensive (>1 km^2) areas of deformed sediment with rigidly deformed layers and oriented stones	Deformed sediment described as cryoturbation with rigidly deformed layers and/or oriented stones	—
Casts of ice crystals	—	Blade-shaped imprints of ice crystals	Imprints of ice crystals (no further description)	—	—
Shattered clasts	—	—	In situ clast, fractured into multiple pieces on subaerial substrate	In situ clast, fractured into multiple pieces	Angular clasts of the same lithology in close proximity
Varves	—	—	—	Rhythmically spaced parallel laminations of alternating composition	Parallel laminations of alternating composition

Note: Adapted from Tindal (2023, tables 2.1 to 2.11). For a full description and an explanation of the evidence categories and ranking, see Tindal (2023, chapter 2).

*Diamictite is not explicitly used as a category of evidence but is used in deposit descriptions. Here, we follow Tindal's (2023) sensu lato use of "diamictite" as a predominantly siliciclastic mudrock with some component of grains that are at least sand-sized, because this covers shifting definitions of diamictite (Flint et al., 1960a, 1960b; Eyles et al., 1983; Moncrieff, 1989; Hambrey and Glasser, 2003). However, we would generally expect a "diamictite" to be matrix supported and to contain pebbles or larger grains.

†Dropstones are defined as outsized clasts in a fine-grained matrix that deform or break laminae beneath them and may show evidence of draping by overlying laminae (see Tindal, 2023, section 2.3.2.2; following Bennett et al., 1996).

§Dropstone evidence classes here follow the pre-Devonian classification of Tindal (2023).

#Lithological groups are igneous, metamorphic, siliciclastic, and carbonate.

TABLE 3. ADAPTATION OF TINDAL'S (2023) TABLE 2.1 DESCRIBING THE FIVE-STAR RATING SCHEME FOR ASSESSING THE POTENTIAL GLACIOGENICITY OF A GIVEN SEDIMENTARY DEPOSIT

Strength	Stars	Relative weight	Definition	Example
Unequivocal	★★★★★	1	No realistic ice-free depositional environment could produce this evidence.	Not applicable: there are currently no five-star Ediacaran deposits.
Strong	★★★★	1/2	No realistic ice-free depositional environment is likely to produce this evidence.	Gaskiers Formation: diamictite and dropstones (★) with very angular to well-rounded clasts (★) from three lithological groups (★★), some of which are faceted or striated (★★★).
Circumstantial	★★★	1/4	This evidence could be produced by specific, but rare, ice-free depositional environments.	Las Ventanas Formation: diamictite and lonestones (★) with angular to subrounded clasts from three lithological groups (★★), some of which are faceted or striated (★★★).
Weak	★★	1/8	Some ice-free depositional environments could produce this evidence.	Fauquier Formation: diamictite with angular to rounded clasts (★) from two lithological groups (★).
Equivocal	★	1/16	Many ice-free depositional environments could produce this evidence.	Bunyeroo Formation: lonestones (★) with clasts of unreported roundness from one lithological group.
Insufficient	☆	0	Many ice-free depositional environments could produce this evidence, and an ice-related origin of the observed features is not supported by the evidence.	Hongtiegou Formation: diamictite with subangular to subrounded clasts from one lithological group.

Note: Here we have added an "insufficient" zero-star rating for deposits that have been interpreted as glaciogenic in the literature but do not meet the one-star evidential threshold following Tindal's (2023) method. We have also added an explicit relative weight column to illustrate the geometric growth in confidence of glaciogenicity with successive star ratings.

TABLE 4. SUMMARY OF THE STAR RATINGS ASSIGNED TO CANDIDATE EDIACARAN GLACIOGENIC DEPOSITS INCLUDED IN PUBLISHED LITERATURE COMPILATIONS

Compilation	Star rating					
	Five	Four	Three	Two	One	Zero
Youbi et al. (2020)	0 (0%)	10 (40%)	10 (40%)	5 (20%)	0 (0%)	0 (0%)
Retallack (2022)	0 (0%)	7 (23%)	7 (23%)	3 (10%)	2 (6%)	12 (39%)
Tindal (2023)*	3 (1%)	62 (28%)	84 (38%)	41 (18%)	16 (7%)	18 (8%)
Wang et al. (2023a, 2023b)	0 (0%)	14 (36%)	16 (41%)	5 (13%)	2 (5%)	2 (5%)
Niu et al. (2024)	1 (2%)	16 (32%)	17 (34%)	5 (10%)	3 (6%)	8 (16%)

Note: Data are presented here as the number (and percentage to nearest 1%) of deposits of each star rating included in each compilation. Most previous compilations include a considerable number of deposits that have weak (two-star or less) sedimentological or geomorphological evidence for glacial conditions. See Tindal (2023), Methods, Table 3, and Supplemental Material (see text footnote 1) for methodology (Supplemental Text S1) and ratings (Supplemental Data S1).

*Tindal's (2023) compilation includes many deposits that are most likely Cryogenian (based on nonradiometric age constraints) in the plausible Ediacaran dataset.

the next (higher) level. In this way, a deposit may be confidently considered glaciogenic if it has either one five-star "unequivocal" line of evidence or several weaker (four-star: "strong;" three-star: "circumstantial;" two-star: "weak;" one-star: "equivocal") lines of evidence (Tables 2 and 3; Tindal, 2023). An additional zero-star "insufficient" category was added here (Table 3), which was previously used but not defined for some deposits that fail to meet the evidence threshold of a one-star deposit (Tindal, 2023).

Each star rating is constructed from described or figured observations of sedimentary and geomorphic features associated with a specific deposit. This scheme is intentionally additive and accumulates lines of evidence in favor of a glaciogenic interpretation because it is designed to be applied to published literature data, where different intensity of study may yield different sets of primary observations for any given deposit (i.e., a greater intensity of study is likely to yield a higher star rating as greater numbers of individually weak lines of evidence accumulate). This methodology is designed to avoid choosing between different reports and therefore retains all reported evidence unless it is specifically refuted. As such, the scheme is vulnerable to false positives, and it should be used to guide interpretations of the potentially glacial origins of a deposit, rather than as a strict diagnostic test. We refer readers to the published thesis for a full description (Tindal, 2023, chapter 2, tables 2.1–2.11).

We consider unreliable those deposits that score less than three out of five stars, meaning that plausibly glaciogenic deposits have "circumstantial" or better evidence that they were formed under glacial influence (Table 3). For some deposits rated less than three stars, the level of described evidence may not accurately reflect the evidence that is available in the field, and so they may be upgraded in the future when further data come to light. Where a deposit was not originally rated by Tindal (2023) and/or where substantial new evidence has been published since his initial assessment, we reviewed the currently available evidence and provided updated ratings for these deposits (see Supplemental Text S1 and Supplemental Data S1).

Ediacaran Paleobiological Data

Our paleobiological dataset is primarily based on the compilations of Boddy et al. (2021) and Bowyer et al. (2024), with additional data from Surprenant and Droser (2024), Muscente et al. (2019), and other primary sources (Supplemental Data S2). The primary age model used to calibrate the paleobiology dataset was age model K from Bowyer et al. (2023, 2024); for deposits older than ca. 550 Ma, the age model followed Yang et al. (2021); for Mistaken Point Ecological Reserve (MPER) data, we followed the original age model of Matthews et al. (2021). Where further radiometric or carbon isotope age controls were available, these were also included within an updated age model (Supplemental Data S2).

We followed Wood et al. (2023) in considering each late Ediacaran biotic assemblage to be characterized by the novel morphotypes or major groups that first appear in that assemblage (Supplemental Data S2). For example, this makes the rangeomorph *Rangea* a component of the Avalon assemblage because rangeomorphs first appeared as a key part of the Avalon assemblage, even though *Rangea* itself is only known from deposits younger than ca. 557 Ma.

We examined raw genus richness and subsampled genus richness using inexact shareholder quorum subsampling (SQS; Alroy, 2010a, 2014) with a quota of 0.4, unweighted collection-based classical rarefaction (UW) with a quota of 8 collections, and occurrence-weighted by-list subsampling (OW) with a quota of 14 occurrences.

The depositional age of the classic White Sea assemblage fossils from South Australia (East Gondwana) is only loosely constrained by the ca. 566 Ma Shuram-correlative Wonoka Formation negative carbon isotope excursion (CIE) below (Yang et al., 2021; Busch et al., 2022, 2023) and the Terreneuvian (early Cambrian) Uratanna and Parachilna Formations above (Betts et al., 2018). The Ediacara Member fossiliferous deposits are typically correlated on the basis of taxonomic similarity with the better constrained deposits of the White Sea region of the East European Platform (Waggoner, 2003; Boag et al., 2016; Muscente et al., 2019; Boddy et al., 2021; Bowyer et al., 2022, 2023, 2024; Evans et al., 2022). We performed our paleontological analyses using the full dataset, and then we performed sensitivity analyses on the dataset excluding South Australia occurrences to understand the impact of the lack of precise dating of these sections.

Software Usage

All quantitative analyses and plots were produced in R (R Core Team, 2021). The divDyn package (Kocsis et al., 2019) was used for paleobiodiversity analyses. The deeptime package (Gearty, 2026) was used to make plots incorporating geological time scale elements. The analysis pipeline also made use of packages within or extensions of the tidyverse suite (Wickham et al., 2019). The code used to produce the analyses and figures is accessible on GitHub: https://github.com/twwh01/Ediacaran_climate_framework.

RESULTS

Recent publications that compiled, compared, or reviewed candidate Ediacaran glaciogenic deposits (Table 1) can be grouped into three broad categories (Fig. S1): (1) those that correlate most glacial evidence to the Gaskiers glaciation (ca. 580 Ma; Youbi et al., 2020); (2) those that argue for two to four short-lived (~1–5 m.y.) glaciations (Linnemann et al., 2018, 2022; Retallack, 2022; Niu et al., 2024); and (3) those that argue for a single, protracted, late Edi-

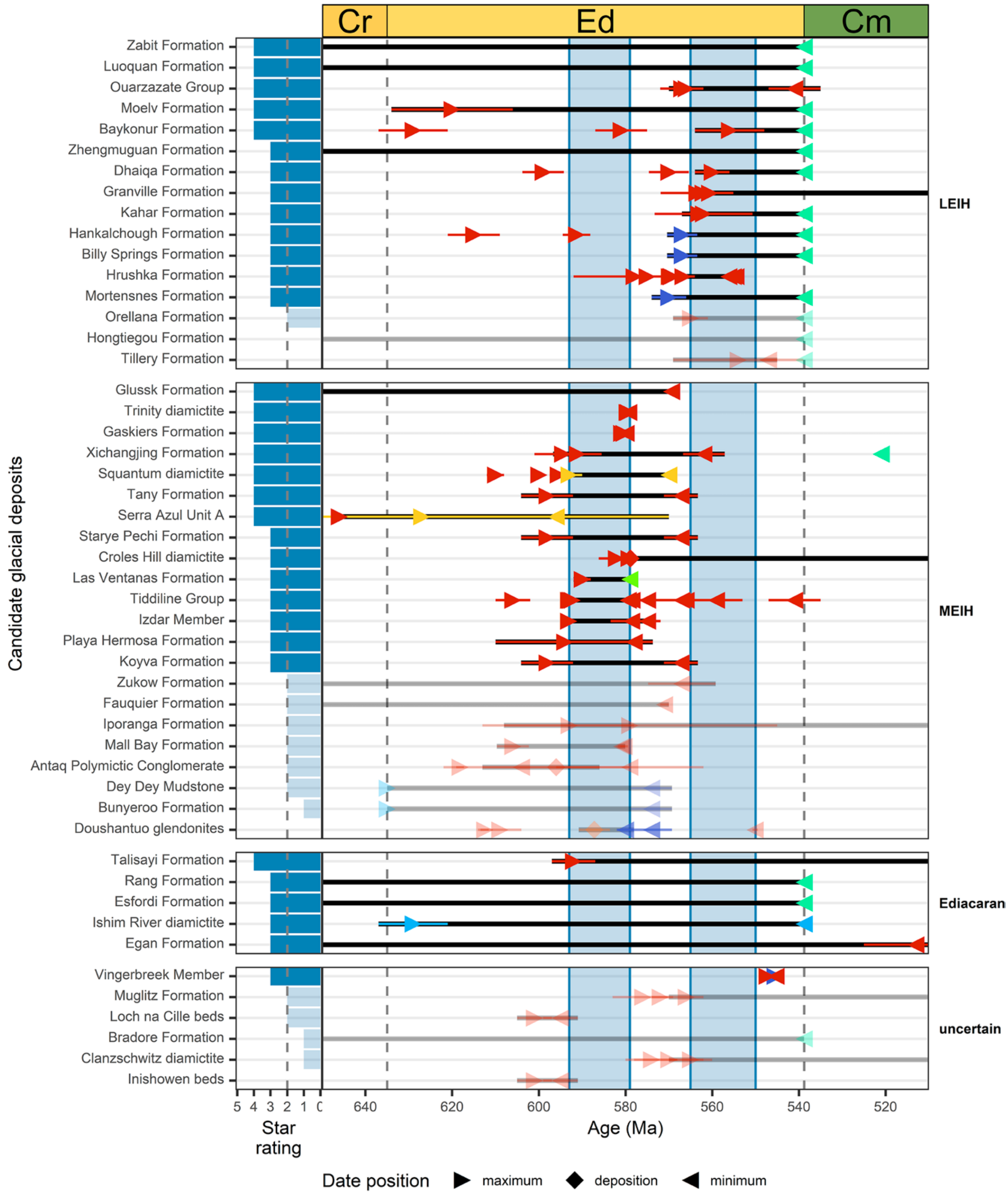
Cr
Ed
Cm
Candidate glacial deposits
Zabit Formation
Luoquan Formation
Ouarzazate Group
Moelv Formation
Baykonur Formation
Zhengmuguan Formation
Dhaiqa Formation
Granville Formation
Kahar Formation
Hankalchough Formation
Billy Springs Formation
Hrushka Formation
Mortensnes Formation
Orellana Formation
Hongtiegou Formation
Tillery Formation
LEIH
Glussk Formation
Trinity diamictite
Gaskiers Formation
Xichangjing Formation
Squantum diamictite
Tany Formation
Serra Azul Unit A
Starye Pechi Formation
Croles Hill diamictite
Las Ventanas Formation
Tiddiline Group
Izdar Member
Playa Hermosa Formation
Koyva Formation
Zukow Formation
Fauquier Formation
Iporanga Formation
Mall Bay Formation
Antaq Polymictic Conglomerate
Dey Dey Mudstone
Bunyeroo Formation
Doushantuo glendonites
MEIH
Talisayi Formation
Rang Formation
Esfordi Formation
Ishim River diamictite
Egan Formation
Ediacaran
Vingerbreek Member
Muglitz Formation
Loch na Cille beds
Bradore Formation
Clanzschwitz diamictite
Inishowen beds
uncertain
5 4 3 2 1 0
Star rating
640 620 600 580 560 540 520
Age (Ma)
Date position
maximum
deposition
minimum
Radiometric: U-Pb
Radiometric: Ar-Ar
CIE
Date type
Radiometric: Re-Os
Biostratigraphy
Radiometric: Pb-Pb
Correlation

Figure 2. Age constraints on candidate Ediacaran glaciogenic deposits grouped by their likely depositional interval. "Ediacaran" deposits are constrained only to the Ediacaran Period; "uncertain" deposits may be Ediacaran in age but have unreliable or disputed age constraints. Thick solid lines show the maximum permitted range for each deposit, including analytical uncertainty where relevant. Symbols show the type of constraint, i.e., whether the date provides a minimum, maximum, or depositional age for a deposit. Deposits that score two stars or less are faded. Vertical blue regions show the likely intervals of the mid-Ediacaran icehouse (MEIH; ca. 593–579 Ma) and the late Ediacaran icehouse (LEIH; ca. 565–550 Ma). Cr—Cryogenian (partial); Ed—Ediacaran; Cm—Cambrian (partial); CIE—carbon isotope excursion. See also Supplemental Data S1 (text footnote 1).

acaran icehouse of ~20–40 m.y. duration (Wang et al., 2023a, 2023b).

Figure 2 shows our updated compilation of candidate mid- to late Ediacaran glaciogenic deposits and our assessment of the strength of evidence for their glaciogenicity. Radiometric age constraints and their uncertainties on the subset of candidate Ediacaran glaciogenic deposits that scored at least three stars are summarized in Figures S2 and S3. The most parsimonious interpretation of our data identifies two icehouse intervals of 10–15 m.y. duration, here termed the mid-Ediacaran icehouse (ca. 593–579 Ma) and the late Ediacaran icehouse (ca. 565–550 Ma), separated by greenhouse intervals termed the late Ediacaran greenhouse (ca. 579–565 Ma) and the terminal Ediacaran greenhouse (ca. 550 Ma to Cambrian). Both intervals are represented by three- or four-star candidate glaciogenic deposits from the central Asian terranes, Baltica, West Gondwana, and East Gondwana (Table S1).

593–579 Ma: Mid-Ediacaran Icehouse (MEIH)

Our compilation demonstrates that there is strong support for Earth's climate being in an icehouse state in the mid-Ediacaran between ca. 593 Ma and ca. 579 Ma (Fig. 2), even when deposits with low confidence of a glaciogenic interpretation (less than three stars) are discounted. This icehouse was previously considered to be a short-lived cold interval of perhaps <1 m.y., characterized as the "Gaskiers glaciation" at ca. 580 Ma (Pu et al., 2016). There is now evidence for icehouse conditions lasting perhaps ca. 5–10 m.y. on Avalonia (Gómez et al., 2024, 2025, 2026; Fitzgerald et al., 2024; Mills et al., 2024), ca. 10 m.y. on the Rio de Plata craton (Oyhantçabal et al., 2007; Mallmann et al., 2007), and ca. 10–15 m.y. on North African Gondwana (Letsch et al., 2018), with a consistent termination age of ca. 579 Ma (Fig. 2).

Often called the "Gaskiers glaciation," here we use the term "mid-Ediacaran icehouse" (MEIH) to emphasize its broader paleogeographical and temporal distribution (Fig. 2). Of the deposits identified in this interval, the Gaskiers Formation and Trinity diamictite (Avalonia; eastern Newfoundland, Canada), both rated four-star deposits (Tindal, 2023), have the tightest age constraints for the termination of glacial activity (Pu et al., 2016). Underlying the Gaskiers Formation on the Avalon Peninsula, eastern Newfoundland, the Mall Bay Formation is only rated a two-star deposit (see the Supplemental Material) but may indicate evidence of cold conditions on Avalonia prior to deposition of the Gaskiers and Trinity diamictites (Fitzgerald et al., 2024). Overlying the Gaskiers Formation, turbidites of the Drook Formation were deposited in similar deep-water slope settings and contain some of the oldest Ediacaran macrofossils (Matthews et al., 2021), but they appear to lack evidence of glacial influence. This is despite much paleontological and stratigraphical research on the upper part of this unit (Hofmann et al., 2008; Matthews et al., 2021), and so this may indicate a sharp change in the local climate regime at ca. 579 Ma (Pu et al., 2016). Strata of the lower Drook Formation may offer insights into the climatic transition at the end of the mid-Ediacaran icehouse. Similarly, there is an emerging record of candidate glaciogenic sedimentary deposits on the Bonavista Peninsula, eastern Newfoundland, from candidate glaciogenic deposits of the Plate Cove East, Monk Bay, and Jones Pond Members and the Mercantile diamictite in the lower Rocky Harbour Group, all below the Trinity diamictite (Gómez et al., 2025, 2026; Mills et al., 2024). Recent radiometric dating suggests that these lower Rocky Harbour Group deposits are younger than 591.3 ± 1.6 Ma (Mills et al., 2017, 2024) and were probably deposited from ca. 589 Ma (Gómez et al., 2025, 2026). Similar to the Trinity diamictite, the Mercantile diamictite has been interpreted as a deglacial facies (Gómez et al., 2025, 2026), which would imply low-altitude glacial activity on Avalonia from ca. 589 Ma. However, further detailed sedimentological assessment (e.g., building on Gómez et al., 2024) is needed to obtain evidence of the glaciogenicity of these units, so they are not yet included in our compilation. The Squantum Member diamictite, Roxbury Conglomerate Formation (Avalonia; northeast United States), has been radiometrically constrained to between ca. 595 Ma and ca. 570 Ma (Thompson and Bowring, 2000; Thompson et al., 2007). Although rated a four-star deposit (Tindal, 2023), the reliability of reports of striated clasts has been called into question, with some studies concluding there is no strong evidence of glaciogenicity (see the Supplemental Material; Dott, 1961; Socci and Smith, 1990; Carto and Eyles, 2012). Nevertheless, the glaciomarine Gaskiers and Trinity diamictites provide strong positive evidence for low-altitude glaciation on Avalonia, terminating at ca. 579 Ma.

Candidate glaciogenic deposits in the Tiddiline Group and Izdar Member (West Gondwana; Morocco), both rated three-star units (Tindal, 2023), were deposited between ca. 593 Ma and ca. 579 Ma (Thomas et al., 2002; Inglis et al., 2004; Blein et al., 2014; Letsch et al., 2018). Letsch et al. (2018) interpreted the diamictites as a combination of terrestrial and marine glaciogenic deposits, providing evidence for proximal glacial activity, whereas they interpreted the laminites with dropstones as reflecting more distal glaciomarine conditions. The repeated alternation of tillites and laminites evidences local waxing and waning of low-altitude land ice on West Gondwana (Letsch et al., 2018). Radiometric dates from Morocco provide perhaps the current best constraints for mid-Ediacaran icehouse glacial onset. U-Pb thermal ionization mass spectrometry (TIMS) dates deriving from igneous zircons from an ignimbrite interbedded with the lower glaciogenic strata and detrital zircons from the lower glaciogenic units themselves across five sections in the Anti-Atlas Mountains constrain the onset of West Gondwanan glaciation to ca. 593 Ma with a youngest volcanic zircon age of 593.12 ± 0.14 Ma and youngest detrital zircon age of 592.68 ± 0.12 Ma (Letsch et al., 2018).

The Las Ventanas and Playa Hermosa Formations (Río de Plata craton; southern Uruguay) are both rated three-star deposits (Tindal, 2023). The Las Ventanas Formation is constrained by radiometric dates to between 590 ± 2 Ma and 579 ± 1.5 Ma (Oyhantçabal et al., 2007; Mallmann et al., 2007), consistent with less precise radiometric ages and acritarch biostratigraphy (Bossi et al., 1993; Sánchez Bettucci and Linares, 1996; Gaucher et al., 2008; Pecoits et al., 2011). The Playa Hermosa Formation is radiometrically constrained to between 594 ± 16 Ma and 578.0 ± 4.3 Ma (Rapalini et al., 2015). The Las Ventanas and Playa Hermosa Formations were deposited in a tectonically active setting with evidence of nonglaciogenic debris-flow deposits, but the candidate glaciogenic deposits include diamictites and fine-grained rhythmites hosting outsized clasts with faceted surfaces (Pecoits, 2003; Pecoits et al., 2008, 2011; Gaucher et al., 2008; Pazos et al., 2011).

The Tany, Koyva, and Starye Pechi diamictites of the Serebryanka and Sylvitsa Groups (Baltica; central Urals, Russia) are constrained between volcanic zircon U-Pb dates 598.1 ± 6.0 Ma (lower Tany Formation) and 567.2 ± 3.9 Ma (the overlying Perevalok Formation; Chumakov, 2011a; Grazhdankin et al., 2011; Maslov et al., 2013; Chumakov et al., 2013). The Tany, Koyva, and Starye Pechi diamictites are variously interbedded with shales and massive quartz-feldspar sandstones as well as minor carbonates (Grazhdankin et al., 2009; Chumakov, 2011a). The geological context indicates deposition on an outer shelf to slope setting, with the diamictites interbedded with various gravity-driven mass flow–derived deposits including flysch, conglomerates, breccias, turbidites, and synsedimentary slumping (Chumakov, 2011a; Maslov et al., 2013; Chumakov et al., 2013). All three units are reported to have evidence indicating a glaciogenic origin, including rare (Ipat'eva *in* Maslov et al., 2013) striated and outsized clasts, and are rated as four-star (Tany) and three-star (Koyva, Starye Pechi) deposits (Tindal, 2023). It is possible, though unproven, that the Starye Pechi Formation was deposited after the mid-Ediacaran icehouse, in the late Ediacaran greenhouse (see "579–565 Ma: Late Ediacaran Greenhouse (LEGH)" section).

Taken together, it is likely that glacial ice had begun to build up by ca. 593 Ma on parts of West Gondwana (Letsch et al., 2018) and by ca. 589 Ma on the peri-Gondwanan terrane of Avalonia (Mills et al., 2017, 2024; Gómez et al., 2025, 2026). We consider 593 Ma to be the current best minimum age for glacial onset on West Gondwana and globally, though future work refining age estimates for deposits on Amazonian West Gondwana, Baltica, and the Altaids may extend this age further back (e.g., Figs. S2 and S3). Ice-sheet growth in different areas was likely diachronous, perhaps over several million years, and there is evidence from West Gondwana, Avalonia, and Baltica of multiple ice-sheet expansions and contractions throughout this interval. The termination of the mid-Ediacaran icehouse is better constrained to ca. 579 Ma across several deposits on West Gondwana and Avalonia, coinciding with the established termination of the "Gaskiers glaciation" (Pu et al., 2016).

579–565 Ma: Late Ediacaran Greenhouse (LEGH)

The late Ediacaran experienced a major perturbation to the carbon cycle, as recorded by the Shuram negative CIE (Burns and Matter, 1993; Xiao and Narbonne, 2020; Yang et al., 2021; Busch et al., 2022), which began no earlier than 575 Ma (Rooney et al., 2020; Yang et al., 2021) and terminated after 566.9 ± 3.5 Ma (Busch et al., 2023). The Shuram CIE has been studied in globally distributed sections and a wide range of depositional settings (Busch et al., 2022; Bergmann et al., 2022; Cantine et al., 2024), yet there are no currently known sections in which a Shuram-like CIE is coincident with a candidate glaciogenic deposit.

However, carbonate olistoliths from the Kernos, Buton, and Starye Pechi Formations have yielded very negative (−15‰ to −10‰) carbon isotope values that were originally interpreted as either diagenetic or resulting from methane or carbon dioxide seeps (Chumakov et al., 2013). We suggest an alternative interpretation: that these carbon isotope values reflect deposition of the olistolith source material during the Shuram CIE. In combination with the 567.2 ± 3.9 Ma radiometric minimum depositional age constraint on the Starye Pechi Formation (Grazhdankin et al., 2011), the olistolith carbon isotope data could provide a depositional window of ca. 574–563 Ma for the Starye Pechi diamictites. If the original interpretation (Chumakov et al., 2013) of the very negative carbon isotope values is correct, then the Starye Pechi Formation may predate the Shuram CIE and be contemporaneous with the mid-Ediacaran icehouse. On current evidence, we consider that pre-Shuram (mid-Ediacaran icehouse; pre–579 Ma), syn-Shuram (late Ediacaran greenhouse; 579–565 Ma), and post-Shuram (late Ediacaran icehouse; post–565 Ma) age assignments are all possible, and further evidence is needed to resolve this question.

There are no further candidate glaciogenic deposits with reasonable depositional age constraints that could plausibly have been deposited between ca. 579 and 565 Ma (Fig. 2). Notably, in sections with near-continuous sedimentation, there is no evidence for glaciation after ca. 579 Ma and before ca. 565 Ma, including in Avalonian sections where glacial deposits were well developed prior to ca. 579 Ma and there is no substantial change in depositional setting (Carto and Eyles, 2011; Pu et al., 2016; Fitzgerald et al., 2024; Mills et al., 2024). Because of the lack of well-constrained evidence for glaciation, we term this interval the "late Ediacaran greenhouse" (LEGH).

565–550 Ma: Late Ediacaran Icehouse (LEIH)

At around ca. 565–560 Ma, a concentration of evidence for land ice returns (Fig. 2) on Gondwana and peri-Gondwanan terranes (Linnemann et al., 2018, 2022). This icehouse interval has been known by various names, but particularly as the "Hankalchough glaciation" (Xiao et al., 2004), the "Baykonurian glaciation" (Chumakov, 2009), or the "Upper Ediacaran Glacial Period" (Linnemann et al., 2022). Here, we use the term "late Ediacaran icehouse" (LEGH) for consistency of terminology and to avoid tying the climate interval to specific deposits.

The Ouarzazate Group diamictites and glacial surfaces (West Gondwana; Morocco) are rated as a four-star deposit (see the Supplemental Material), with a maximum depositional age of 566 ± 4 Ma (Blein et al., 2014), therefore likely postdating the recovery of the Shuram CIE. The Kahar Formation diamictite (East Gondwana; Iran), rated as a three-star deposit (Tindal, 2023), has a radiometrically constrained maximum depositional age of 563.1 ± 3.9 Ma and a formal minimum age of 538.8 Ma informed by overlying earliest Cambrian trace fossils (Etemad-Saeed et al., 2016). The Kahar diamictite has also been suggested to be older than 550.3 ± 3.6 Ma based on the younger age population of detrital zircons in an overlying sample (Etemad-Saeed et al., 2016). The Dhaiqa Formation diamictite (East Gondwana; Saudi Arabia), rated as a three-star deposit (Tindal, 2023), is younger than 560 ± 4 Ma and underlies candidate Ediacaran fossils (Miller et al., 2008; Vickers-Rich et al., 2012).

The eponymous Baykonur Formation is a four-star deposit (Tindal, 2023) that crops out in the Middle Tianshan area, part of the late Neoproterozoic–early Paleozoic central Asian terranes, and has only recently been radiometrically dated: Laser ablation–inductively coupled plasma–mass spectrometry (LA-ICP-MS) detrital zircon U-Pb dates from samples in the upper Baykonur Formation in Kyrgyzstan support a late Ediacaran (ca. 555 Ma) maximum depositional age, with two samples dated at 581 ± 6 Ma and 556 ± 8 Ma (youngest single-grain date of 554 ± 10 Ma; Alexeiev et al., 2025). Acritarch biostratigraphy indicates an early Cambrian age for the overlying shales and limestones, with trilobite fossils found further up the succession (Chumakov, 2011b). These data support the long-standing but until recently unproven hypothesis that the Baykonur Formation diamictite was deposited in the late Ediacaran.

Several candidate glaciogenic deposits in the paleoterranes of present-day northern China have poor age constraints but were likely deposited between ca. 565 Ma and ca. 550 Ma (Xiao et al., 2004; Shen et al., 2007, 2010; Zhou et al., 2019; Le Heron et al., 2019; Wang et al., 2021a; Wang et al., 2023b). The Luoquan and Zhengmuguan Formations (North China craton; China) are four-star (Tindal, 2023) and three-star (see the Supplemental Material) deposits, respectively. The Luoquan and Zhengmuguan Formations are likely correlatives of each other (Le Heron et al., 2019; Wang et al., 2021a) and were deposited below the first occurrences of the late Ediacaran tubular taxon *Shaanxilithes* in the conformably overlying Dongpo and Tuerkeng Formations, respectively (Shen et al., 2007; Zhou et al., 2019; Wang et al., 2021a). Similarly, the poorly documented Hongtiegou Formation diamictite (Qaidam block; China; see the Supplemental Material) was deposited below occurrences of *Charnia* and *Shaanxilithes* taxa in the Zhoujieshan Formation (Shen et al., 2010; Pang et al., 2021; Wang et al., 2022). The Luoquan, Zhengmuguan, and Hongtiegou Formations unconformably overlie Mesoproterozoic sedimentary deposits but are conformable with their overlying, Ediacaran fossil–bearing units (Shen et al., 2007, 2010; Wang et al., 2021a). The Hankalchough Formation (Tarim block; China) is a three-star deposit (see the Supplemental Material) that occurs at least 65 m stratigraphically above the recovery limb of an extreme negative CIE in the Shuiquan Formation that has been correlated with the Shuram CIE (Xiao et al., 2004; Wang et al., 2023a). The maximum depositional age of the Hankalchough Formation is therefore taken as the minimum age of the Shuram CIE recovery: 566.9 ± 3.5 Ma (Busch et al., 2023). The overlying Xishanblaq Formation hosts earliest Cambrian acritarchs, which provide a minimum Cambrian age constraint on the Hankalchough Formation (Xiao et al., 2004; Yao et al., 2005).

The Mortensnes Formation diamictite (Baltica; Norway) is a three-star deposit (Tindal, 2023) lacking precise radiometric dates, but it is also constrained by a likely Shuram-equivalent CIE below (Halverson et al., 2005; Rice et al., 2011) and Ediacaran macrofossils above (Högström et al., 2013; McIlroy and Brasier, 2017; Jensen et al., 2018; Agić et al., 2024). It is likely that the Mortensnes Formation was deposited between the Shuram CIE and the terminal Ediacaran. The Hrushka Formation diamictite (Baltica, Moldova and Ukraine) is a three-star deposit bracketed by radiometric constraints of ca. 567 Ma below and ca. 557 Ma above (both from detrital zircon populations; Środoń et al., 2023), but the isotopic composition of detrital zircons in the Hrushka Formation better supports an alluvial than glaciogenic interpretation (Francovschi et al., 2024).

Four candidate glaciogenic deposits have been identified across the peri-Gondwanan Cadomia microcontinent (Linnemann et al., 2018, 2022). Diamictites from the Müglitz Formation (Weesenstein Group) and Clanzschwitz Group Member 3 (both Cadomia; Germany) are rated as two and one-star deposits, respectively (see the Supplemental Material), and were considered to be likely younger than 562 ± 5 Ma (Linnemann et al., 2018). However, recent work has indicated a nonglacial origin for these units as well as a considerably revised depositional age of late Cambrian to Ordovician based on U-Th-Pb monazite dates (Kühnemann et al., 2025) and ichnofossil evidence (Meinhold et al., 2025). The Granville Formation diamictites (Cadomia; France), rated as a three-star deposit (Tindal, 2023), are younger than 562.1 ± 3.1 Ma, with the upper diamictite younger than 560.6 ± 3.3 Ma (Linnemann et al., 2022). The Orellana Formation (Cadomia; Spain), rated as a two-star deposit (Tindal, 2023) and not universally regarded as glaciogenic (Palacios, 2024), is younger than 565 ± 4 Ma (Linnemann et al., 2018) and is found unconformably below late Ediacaran fossil–bearing carbonates (Álvaro et al., 2019; Palacios, 2024). Overall, the evidence for late Ediacaran glaciation across Cadomia in the ca. 565–550 Ma interval is weak in comparison to that on paleocontinental Gondwana and the terranes of northern China.

Where there is depositional continuity above the late Ediacaran icehouse candidate glaciogenic deposits, late Ediacaran fossils are commonly found in the overlying strata (Shen et al., 2007, 2010; Vickers-Rich et al., 2012; Högström et al., 2013; Jensen et al., 2018; Wang et al., 2021a, 2022; Agić et al., 2024), demonstrating that this icehouse terminated before the end of the Ediacaran. Less well constrained than the mid-Ediacaran icehouse, the late Ediacaran icehouse probably commenced after the Shuram CIE recovery, likely between 565 Ma and 560 Ma, and terminated before the end of the Ediacaran Period, likely ca. 550 Ma (Xiao et al., 2004; Miller et al., 2008; Chumakov, 2009; Vickers-Rich et al., 2012; Etemad-Saeed et al., 2016; Linnemann et al., 2018, 2022; Agić et al., 2024).

550–539 Ma: Terminal Ediacaran Greenhouse

There is scant evidence of glaciation in the terminal Ediacaran, likely after ca. 550 Ma. The only temporally well-constrained candidate glaciogenic deposit known from this interval was the Vingerbreek Member of the Nudaus Formation, Nama Group (Kalahari craton, East Gondwana; Namibia and South Africa) and the associated basal Vingerbreek Unconformity (Schwellnus, 1941; Kröner and Germs, 1971; Kröner, 1981; Germs and Gaucher, 2012; Zieger-Hofmann et al., 2022), which are together rated as a three-star deposit (Tindal, 2023). The Vingerbreek Member and Unconformity are radiometrically constrained to between 547.36 ± 0.23 Ma (Bowring et al., 2007) and 545.27 ± 0.11 Ma (Nelson et al., 2022).

The Vingerbreek Unconformity has only been found in parts of the southern Nama Basin (the Zaris and possibly the Vioolsdrif subbasins), not in the Witputs subbasin to the north (Kröner, 1981; Germs and Gaucher, 2012; Zieger-Hofmann et al., 2022). The Vingerbreek Member basal diamictite was deposited in wide channels in the unconformity surface, which have been interpreted as deriving from fluvial or submarine mass-flow erosion processes; both far-field glacio-eustasy and tectonism have been proposed as potentially responsible for lowering base level (Martin, 1965; Kröner, 1981; Germs and Gaucher, 2012). The grooves and surface polish on some channel flanks have been interpreted as deriving from glacier–rock (Schwellnus, 1941; Germs and Gaucher, 2012; Zieger-Hofmann et al., 2022) or sea ice–rock (Martin, 1965; Kröner, 1981) interactions, though similar features also form from mass-flow and rock avalanche erosion processes (Hambrey and Harland, 1981a; Hu and McSaveney, 2018). The diamictite deposits are better described as conglomerates and breccias (Germs and Gaucher, 2012) and have been interpreted as fluvial or submarine current–derived deposits, including in studies that found glacial action at least partly responsible for the unconformity (Kröner, 1981; Germs and Gaucher, 2012). In northwest South Africa, the diamictite grades into turbidites (Zieger-Hofmann et al., 2022). Recent restudy of candidate glaciogenic deposits in the Vingerbreek Member has suggested that the likely glaciogenic components are a combination of misidentified Dwyka Formation deposits of late Carboniferous to Permian age and nonglaciogenic Ediacaran deposits (Baillie et al., 2025). The Vingerbreek Member and Unconformity therefore provide, at best, only circumstantial, stratigraphically and spatially isolated evidence for glacial ice. Further fieldwork is required to determine the depositional context of the Vingerbreek Unconformity and Vingerbreek Member, and it stands as a test of our hypothesis that the ca. 550–545 Ma interval was characterized by a greenhouse climate.

Elsewhere, the terminal Ediacaran lacks any signs of glaciation, and we therefore use the term "terminal Ediacaran greenhouse" for this interval. Similar to previous compilations of climatically sensitive lithologies (Boucot et al., 2013; Wong Hearing et al., 2021), we do not find evidence of well-dated glacial sedimentary deposits in either the terminal Ediacaran or early Cambrian Periods.

Climate and the Ediacaran Biosphere

Our analysis indicates that the mid- to late Ediacaran climate was characterized by two icehouse intervals (ca. 593–579 Ma and ca.

Figure 3. Representative late Ediacaran fossils of the Avalon, White Sea, and Nama biotic assemblages. Scale bars = 10 mm unless otherwise stated; photographed scale bar increments are centimeter and millimeter. Nama (left to right): *Charnia masoni*, NIGP 161628, Shibantan Member (Dengying Formation), Wuhe, South China, scale bar = 10 cm; *Helicolocellus cantori*, NIGP 176531, Shibantan Member (Dengying Formation), Wuhe, South China; *Pteridinium*, Aar Member, Farm Aar, Namibia; *Namacalathus*, Urusis Formation, Farm Swartpunt, Namibia; *Corumbella werneri*, Tamengo Formation, Corumba region, Brazil; burrows in carbonates, Shibantan Member (Dengying Formation), Wuhe, South China. White Sea (left to right): *Charnia masoni* (incomplete), Verkhovka Formation, Solza River, Russia; *Dickinsonia costata*, SAM P49355, Ediacara Member (Rawnsley Quartzite), Flinders Ranges, South Australia; *Kimberella quadrata*, PIN 3993/5106, Vendian Group, Zimnie Gory locality, White Sea coast, Russia; *Tribrachidium*, SAM P12898, Ediacara Member (Rawnsley Quartzite), Flinders Ranges, South Australia; *Funisia dorothea*, Ediacara Member, South Australia; *Helminthoidichnites* trace fossils, SAM P42142, Ediacara Member, Flinders Ranges (Rawnsley Quartzite), South Australia. Avalon (left to right): *Charnia masoni* (holotype), New Walk Museum, Leicester, Bradgate Formation, Charnwood Forest, UK; *Haootia quadriformis* (holotype), NFM F-994, Fermeuse Formation, Bonavista Peninsula, Newfoundland, Canada; *Bradgatia*, ROM 36500, Conception Group, Mistaken Point Ecological Reserve (MPER), Newfoundland, Canada; *Fractofusus andersoni*, Briscal Formation, MPER, Newfoundland, Canada; surface locomotory trace fossil, Mistaken Point Formation, MPER, Newfoundland, Canada. Abbreviations: NIGP—Nanjing Institute of Geology and Palaeontology, Nanjing, China; ROM—Royal Ontario Museum, Toronto, Ontario, Canada; NFM—The Rooms Provincial Museum, St. John's, Newfoundland, Canada; SAM—South Australia Museum, Adelaide, Australia; PIN—Palaeontological Institute, Moscow, Russia.

565–550 Ma) and two greenhouse intervals (ca. 579–565 Ma and ca. 550–539 Ma). Independent of our analysis, the late Ediacaran biosphere has been characterized by three distinct marine biotic assemblages (Figs. 3 and 4; Table 5), with their different taxonomic compositions governed by some combination of environmental and evolutionary controls (Waggoner, 2003; Grazhdankin, 2004; Gehling and Droser, 2013; Boag et al., 2016, 2024; Muscente et al., 2019; Evans et al., 2022). To test whether biotic turnover was coincident with climatic shifts, we examined diversity dynamics over this interval, mindful that the assemblages are typically found in different paleogeographic regions and depositional settings, as well as time intervals (Waggoner, 2003; Boag et al., 2016, 2024; Muscente et al., 2019; Boddy et al., 2021; Bowyer et al., 2022, 2023, 2024; Evans et al., 2022). Because of the substantial contribution of geological and societal biases in the current Ediacaran fossil record (taxonomic richness largely follows sampling intensity; Fig. 5; Bowyer et al., 2024), it is generally more instructive to consider taxonomic composition than taxonomic richness. Nevertheless, some biodiversity signals do appear to be robust to sampling biases (Fig. 5).

Avalon Biotic Assemblage

Diverse communities of the Ediacaran macrobiota belonging to the Avalon biotic assemblage first appear in deep-marine siliciclastic deposits between ca. 579 Ma and ca. 575 Ma (Fig. 4), after the mid-Ediacaran icehouse and before the Shuram CIE (Pu et al., 2016; Matthews et al., 2021; Yang et al., 2021; Boag et al., 2024; Bowyer et al., 2024). The Avalon biotic assemblage comprises predominantly sessile benthic taxa including frondose and non-frondose morphologies, some of which likely stood up in the water column whereas others reclined on the seafloor (Gehling and Narbonne, 2007), alongside candidate cnidarians (e.g., Liu et al., 2014a, 2015; Dunn et al., 2022), and rare trace fossils (Liu et al., 2010, 2014b). This assemblage reaches an apparent acme in diversity in deep-marine settings ca. 565 Ma (Matthews et al., 2021; Boag et al., 2024), coincident with the end of the late Ediacaran greenhouse and the transition into the late Ediacaran icehouse (Fig. 4). The post–560 Ma fate of the deep-water Ediacaran biota remains uncertain due to the scarcity of deep-marine siliciclastic deposits after this time (Bowyer et al., 2024), but the recent discovery of the age of the "EM Coombs" fossil surface in Avalonian Newfoundland suggests that Avalon-type assemblages may have persisted in marine settings until at least ca. 551 Ma (McIlroy et al., 2026).

Depauperate communities of the Avalon biotic assemblage are known from shallow-marine settings on Avalonia (Cope, 1977, 1983; Gehling et al., 2000; Menon et al., 2013; Menon, 2015; Hawco et al., 2021) and Laurentia (Hofmann et al., 1983; Narbonne and Hofmann, 1987; Pyle et al., 2004; Moynihan et al., 2019) after, but not before or during, the Shuram CIE (ca. 574–566 Ma; Matthews et al., 2021; Boag et al., 2024; Clarke et al., 2024). The post-Shuram CIE shallow-marine Avalon biotic assemblages are differentiated from the shallow-marine White Sea biotic assemblages more by the absence of taxa rather than their presence. There are no taxa exclusive to the Avalon biotic assemblage in these shallow-water deposits. The tubular fossils, dickinsoniomorphs, bilaterialomorphs, and radial morphogroups that are ubiquitous in younger White Sea biotic assemblage deposits are absent from the shallow-marine Avalon biotic assemblage sites, as well as from coeval post-Shuram deeper-marine sites (Fig. S4; Narbonne et al., 2014; Noble et al., 2015; Carbone et al., 2015; Kenchington et al., 2018; Boag et al., 2024; Clarke et al., 2024).

The low number and diversity of shallow-water occurrences of the Avalon biotic assemblage may be an artifact of environmental specificity, preservation, or collection bias, but it is notable that no macrofossils have been recovered from pre-Shuram CIE shallow-marine rocks with suitable sedimentology for fossil preservation, even where such rocks have been intensively studied (Boag et al., 2024). Although the scarcity of deep-marine siliciclastic deposits after ca. 560 Ma may explain the apparent loss of the deep-water Avalon biotic assemblage, there is no concomitant absence of pre- and syn-Shuram CIE shallow- and mid-depth marine carbonate and siliciclastic deposits (Bowyer et al., 2024); i.e., there are older strata that could have preserved a shallow-marine Avalon biotic assemblage if it were present (such as the shallow-marine facies of the Nadaleen and Gametrail Formations, NW Canada; Boag et al., 2024). This observation lends support to the idea that the majority of Avalon assemblage taxa belonged to a deep-water biotope (Boag et al., 2016, 2024; Bowyer et al., 2024), with some components (e.g., *Charnia* and *Charniodiscus*) being environmentally tolerant generalist taxa that were capable of inhabiting shallower marine settings in the later Ediacaran (Grazhdankin, 2014; Boag et al., 2024). Here we suggest that a ca. 565–560 Ma interval of global cooling at the onset of the late Ediacaran icehouse allowed more generalist taxa of the otherwise deep-water-adapted Avalon assemblage to colonize cooling shallow-marine environments.

White Sea Biotic Assemblage

In situ paleocommunities of White Sea biotic assemblage taxa are found in shallow-marine settings, above storm weather wave base and predominantly above fair weather wave base (e.g., Grazhdankin, 2004; McMahon et al., 2020) from before 557 Ma until at least 553 Ma (Martin et al., 2000; Fedonkin et al., 2012; Grazhdankin, 2014; Yang et al., 2021; Bowyer et al., 2022, 2024). Our analysis places this range within the late Ediacaran icehouse. The White Sea biotic assemblage is defined by the appearance of new morphogroups (Fig. S4), including bilaterialomorphs, radialomorphs, and tubular forms, which occur alongside a few persistent Avalon-type taxa (Fig. 4; Table 5; Martin et al., 2000; Narbonne, 2005; Fedonkin et al., 2012; Grazhdankin, 2014; Muscente et al., 2019; Surprenant and Droser, 2024). The first step change in trace fossil diversity is associated with this interval: Rare trace fossils older than 560 Ma are stratigraphically isolated simple surface traces (Liu et al., 2010, 2014b), but from at least 557 Ma onward, various horizontal burrows and trails created by candidate bilaterians are found in shallow-marine deposits (Fig. S4). Novel morphogroups are found in shallow-marine strata deposited during the latter part of the late Ediacaran icehouse (ca. 560–550 Ma) but not before ca. 560 Ma (see "Avalon Biotic Assemblage" section; Boag et al., 2024; Clarke et al., 2024). By raw taxonomic richness, the White Sea is the most diverse of the three biotic assemblages, and, although the Ediacaran fossil record is strongly affected by sampling biases, the White Sea diversity peak may be robust under some subsampling methods designed to mitigate such biases (Fig. 5), and it is robust to the inclusion and exclusion of data from South Australian sites, which have only loose age constraints (cf. Fig. 4 and Fig. S5; cf. Fig. 5 and Fig. S6).

Nama Biotic Assemblage

The Nama biotic assemblage is the youngest of the three assemblages, and it is found in shallow-marine carbonate and siliciclastic deposits younger than ca. 550.5 Ma (Darroch et al., 2015; Muscente et al., 2019; Xiao et al., 2021; Wood et al., 2023; Boag et al., 2024) up to the base of the Cambrian (Linnemann et al., 2019; Bowyer et al., 2022, 2023, 2024; Nelson et al., 2022; Wood et al., 2023; Runnegar et al., 2024). It is characterized by the diversification of trace fossils, particularly vertical burrows, and the appearance of biomineralized tubular taxa, which are found only in deposits younger than ca. 550.5 Ma (Wood et al., 2023; Surprenant and Droser, 2024). Some White Sea–type taxa, including dickinsoniomorphs and ernietomorphs (Xiao et al., 2021; Wang et al., 2021b; Wood et al., 2023), and Avalon-type taxa, including arboreomorphs and rangeomorphs (Xiao et al., 2021; Wu et al., 2024b), are found alongside novel Nama morphogroups in shallow-marine deposits from this interval. Recent work has shown that there is considerable overlap in the depositional settings of major White Sea and Nama biotic assemblage sites, increasing the likelihood that the differences in assemblage composition reflect a biological change rather than a change in the environments being sampled (McMahon et al., 2020; Evans et al., 2022; O'Connell et al., 2025). In our analysis, the Nama biotic assemblage is coincident with the terminal Ediacaran greenhouse.

Summary

The Ediacaran macrobiota was initially restricted to deep-marine settings during the late Ediacaran greenhouse (Avalon assemblage, ca.

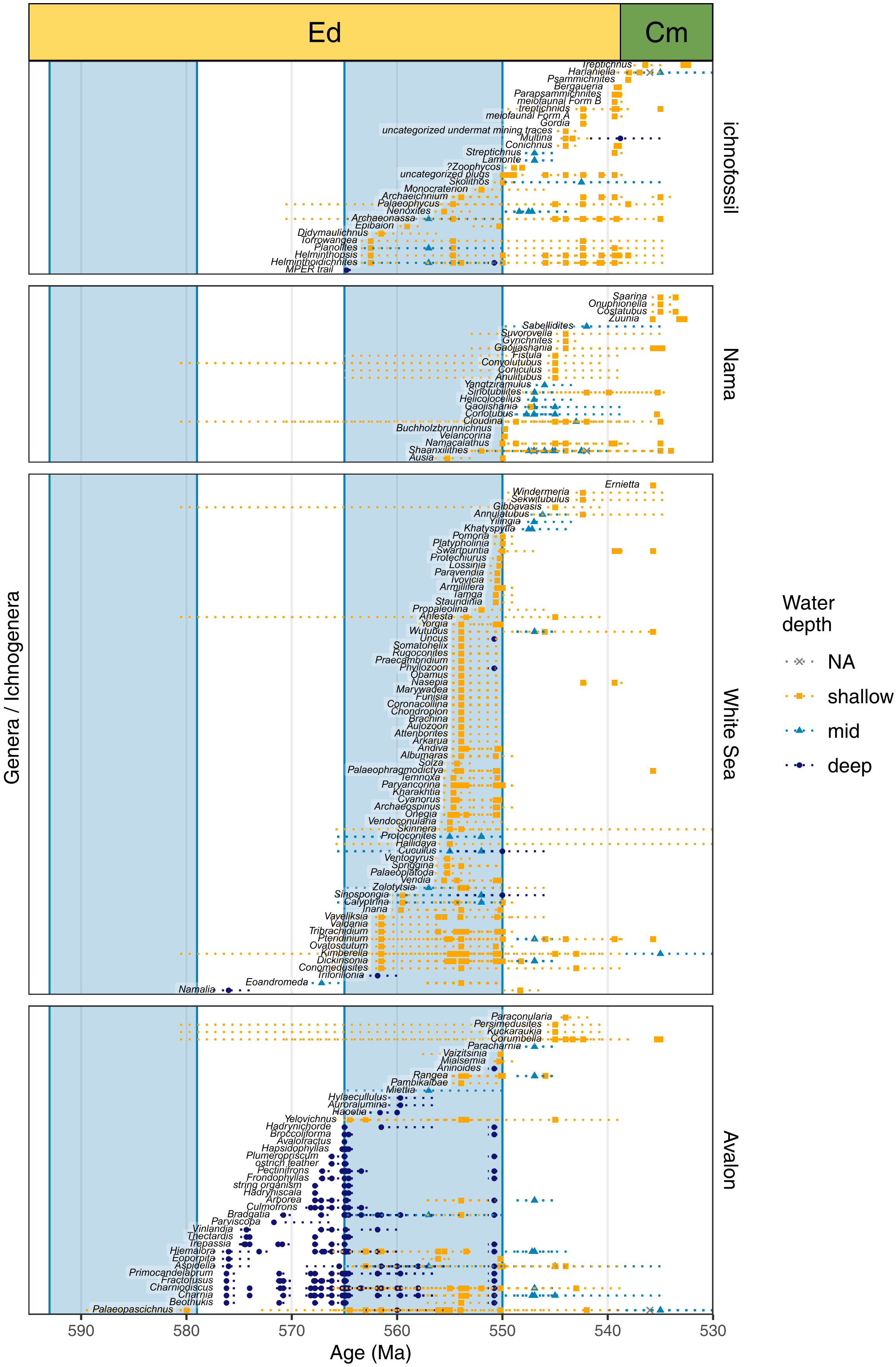
Ed
Cm
ichnofossil
Treptichnus
Harlaniella
Psammichnites
Bergaueria
Parapsammichnites
meiofaunal Form B
treptichnids
meiofaunal Form A
Gordia
uncategorized undermat mining traces
Multina
Conichnus
Streptichnus
Lamonte
?Zoophycos
uncategorized plugs
Skolithos
Monocraterion
Archaeichnium
Palaeophycus
Nenoxites
Archaeonassa
Epibaion
Didymaulichnus
Torrowangea
Planolites
Helminthopsis
Helminthoidichnites
MPER trail
Nama
Saarina
Onuphionella
Costatubus
Zuunia
Sabellidites
Suvorovella
Gyrichnites
Gaojiashania
Fistula
Convolutubus
Conicculus
Anulitubus
Yangtziramulus
Sinotubulites
Helicolocellus
Gaojishania
Conotubus
Cloudina
Buchholzbrunnichnus
Velancorina
Namacalathus
Shaanxilithes
Ausia
White Sea
Ernietta
Windermeria
Sekwitubulus
Gibbavasis
Annulatubus
Yilingia
Khatyspytia
Pomoria
Platypholinia
Swartpuntia
Protechiurus
Lossinia
Paravendia
Ivovicia
Armillifera
Tamga
Stauridinia
Propaleolina
Anfesta
Yorgia
Wutubus
Uncus
Somatohelix
Rugoconites
Praecambridium
Phyllozoon
Obamus
Nasepia
Marywadea
Funisia
Coronacollina
Chondroplon
Brachina
Aulozoon
Attenborites
Arkarua
Andiva
Albumares
Solza
Palaeophragmodictya
Temnoxa
Parvancorina
Kharakhtia
Cyanorus
Archaeaspinus
Onegia
Vendoconularia
Skinnera
Protoconites
Hallidaya
Cucullus
Ventogyrus
Spriggina
Palaeoplatoda
Vendia
Zolotytsia
Sinospongia
Calyptrina
Inaria
Vaveliksia
Valdainia
Tribrachidium
Pteridinium
Ovatoscutum
Kimberella
Dickinsonia
Conomedusites
Triforillonia
Eoandromeda
Namalia
Avalon
Paraconularia
Persimedusites
Kuckaraukia
Corumbella
Paracharnia
Vaizitsinia
Mialsemia
Aninoides
Rangea
Pambikalbae
Miettia
Hylaecullulus
Auroralumina
Haootia
Yelovichnus
Hadrynichorde
Broccoliforma
Avalofractus
Hapsidophyllas
Plumeropriscum
ostrich feather
Pectinifrons
Frondophyllas
string organism
Hadryniscala
Arborea
Culmofrons
Bradgatia
Parviscopa
Vinlandia
Thectardis
Trepassia
Hiemalora
Eoporpita
Aspidella
Primocandelabrum
Fractofusus
Charniodiscus
Charnia
Beothukis
Palaeopascichnus
590
580
570
560
550
540
530
Age (Ma)
Genera / Ichnogenera
Water depth
NA
shallow
mid
deep

Figure 4. Temporal distribution of Ediacaran fossil occurrences, with blue-shaded mid-Ediacaran (ca. 593–579 Ma) and late Ediacaran (565–550 Ma) icehouse climate states as inferred from well-dated glaciogenic deposits (Fig. 2). Paleobiological data are after Matthews (2015), Matthews et al. (2021), Boddy et al. (2021), Bowyer et al. (2023, 2024), Surprenant and Droser (2024), and references therein. Taxa are grouped into assemblages following their morphogroup assignments (sensu Wood et al., 2023). Colors and shapes represent inferred water depth of each occurrence. Ed—Ediacaran (partial); Cm—Cambrian (partial); NA—unknown; MPER—Mistaken Point Ecological Reserve. Dashed lines show the age uncertainty of each occurrence, not age range. See also Supplemental Data S2 and Figure S5 (text footnote 1).

575–565 Ma; Boag et al., 2024); from the beginning of the late Ediacaran icehouse (ca. 565 Ma), elements of the Avalon assemblage appear to have colonized shallow-marine settings. The first step change in high-level taxonomic composition of the Ediacaran biosphere, including the advent of bilaterians and nonmineralized tubes, occurred early in the late Ediacaran icehouse (before ca. 557 Ma) with the appearance of White Sea biotic assemblage morphogroups. This step change is underlined by the Ediacaran peak origination rate across the Avalon–White Sea transition, and the subsequent White Sea peak in taxonomic richness (Fig. 5). A second step change in high-level taxonomic composition accompanied the transition from the late Ediacaran icehouse to the terminal Ediacaran greenhouse (ca. 550 Ma) with the appearance of biomineralizing taxa and vertical burrowing in shallow-marine settings.

Similar to previous studies, our dataset shows low genus-level taxonomic similarity (Table S8) of time-separated assemblages when split at 565 Ma or 560 Ma (Avalon/White Sea) and at 550 Ma (White Sea/Nama). The Jaccard (J) and Dice-Sørensen (D-S) similarity indices are consistently low for both Avalon/White Sea (565 Ma: $J = 0.25$, $D\text{-}S = 0.40$; 560 Ma: $J = 0.26$, $D\text{-}S = 0.42$) and White Sea/Nama (565 Ma: $J = 0.17$, $D\text{-}S = 0.30$; 560 Ma: $J = 0.19$, $D\text{-}S = 0.32$) interval comparisons, but the Simpson similarity index (S) shows higher values for the Avalon/White Sea interval (565 Ma: $S = 0.89$; 560 Ma: $S = 0.67$; $S = 0.42$ for both 565 Ma and 560 Ma White Sea/Nama comparisons). The low values of all similarity indices between the White Sea and Nama intervals, split at 550 Ma, support the hypothesis of a biotic turnover around this time. The higher Simpson similarity index for the Avalon/White Sea comparison for both a 565 Ma and 560 Ma split suggests that the Avalon interval assemblage is a taxonomic subset of the White Sea interval assemblage, partly driven by the persistence of some Avalon assemblage taxa until at least 551 Ma, consistent with the recent discovery of the ca. 551 Ma age of the "EM Coombs" fossil surface in Avalonian Newfoundland (McIlroy et al., 2026). The difference in Simpson coefficient between the 565 Ma and 560 Ma divisions reflects (1) the loss of some Avalon assemblage taxa between 565 Ma and 560 Ma and (2) the diminished difference in taxonomic richness (565 Ma split: 28 vs. 96 genera; 560 Ma split: 39 vs. 86 genera). The low Jaccard and Dice-Sørensen indices between each of the assemblages reflect the presence of taxa in each interval that are absent from the preceding or following interval; i.e., there are many White Sea taxa not found before 560 Ma or after 550 Ma, and most Nama taxa are not found before 550 Ma. There is therefore quantitative support for an increase in genus-level diversity at ca. 560 Ma, and a genus-level turnover at ca. 550 Ma (Table S8), notwithstanding environmental or geographic controls on faunal composition (Waggoner, 2003; Grazhdankin, 2004; Gehling and Droser, 2013; Boag et al., 2016, 2024; Muscente et al., 2019; Boddy et al., 2021; Evans et al., 2022).

Considering only shallow-water occurrences (from strata deposited above storm wave base), the small numbers of taxa shared among the shallow-water Avalon, White Sea, and Nama communities support discrete episodes of faunal turnover (extinctions and radiations) in the shallow-marine realm across the late Ediacaran (Fig. 4). There appear to be distinct assemblages of morphogroups in the late Ediacaran (Waggoner, 2003; Boag et al., 2016; Muscente et al., 2019; Evans et al., 2022) that are separated in time, demarcated by the prevailing climate regime (Fig. 4).

DISCUSSION

Timing of Ediacaran Climate Change

Evidence in the mid- to late Ediacaran sedimentary record is consistent with two intervals of persistent but fluctuating low-altitude ice sheets: the mid-Ediacaran icehouse (ca. 593–579 Ma) and the late Ediacaran icehouse (ca. 565–550 Ma; Fig. 2; Figs. S2 and S3). Our analysis, based on a systematic treatment of all so-far-reported candidate mid- and late Ediacaran glaciogenic deposits, does not support previous hypotheses of either one long (e.g., Wang et al., 2023a, 2023b) or two to four very short (<5 m.y.; Retallack, 2022; Linnemann et al., 2022; Niu et al., 2024) icehouse intervals.

The initiation of the mid-Ediacaran icehouse is moderately well constrained by radiometrically dated deposits in North Africa (ca. 593 Ma; Letsch et al., 2018) and Avalonia (ca.

TABLE 5. SUMMARY OF THE MAIN LATE EDIACARAN BIOTIC ASSEMBLAGES

Assemblage	Age range*	Depositional setting(s)	Morphogroups and innovations
Avalon	<579 Ma to 565 Ma	Deep-marine basin to shelf (Narbonne et al., 2014; Noble et al., 2015; Matthews et al., 2021), lacking shallow-marine occurrences (Boag et al., 2024).	Complex macroscopic organisms; mostly frondose morphologies; no tubular taxa.
	565 Ma to <560 Ma	Deep-marine shelf to basin (Narbonne et al., 2014; Noble et al., 2015; Carbone et al., 2015; Matthews et al., 2021; Boag et al., 2024), and shallow marine, above storm wave base (Cope, 1977, 1983; Pauley, 1991; Liu, 2011; Clarke et al., 2024). Persisting in marine settings until ca. 551 Ma (McIlroy et al., 2026).	Complex macroscopic organisms; frondose morphologies; discoidal fossils both of probable frond holdfasts and individual discoidal organisms; rare simple surface trace fossils; candidate cnidarians; no or very few tubular taxa (Carbone et al., 2015); matgrounds in shallower settings.
White Sea	<560 Ma to >550 Ma	Marine offshore shelf to shallow shoreface (Grazhdankin, 2004; Boag et al., 2016, 2024; McMahon et al., 2020), most likely spanning all settings from near storm wave base to the intertidal zone (McMahon et al., 2020).	Bilaterialomorphs; first erniettomorphs; various radialomorphs; abundant nonmineralized tubular fossils (Surprenant and Droser, 2024); increasingly diverse simple trace fossils; fewer frondose fossils.
Nama	<550 Ma to 538.8 Ma	Marine offshore (open-marine) inner shelf to reef (Boag et al., 2016, 2024; Amorim et al., 2020; Xiao et al., 2021; Wood et al., 2023; O'Connell et al., 2025), including sites in shallow settings above storm wave base (Boag et al., 2016, table 6; Xiao et al., 2020).	Biomineralized and soft-bodied tubular fossils (Surprenant and Droser, 2024); increasingly diverse and complex trace fossils; few new frondose fossils; erniettomorphs become more prominent; candidate sponges.

*The symbols ">" and "<" are used to indicate minimum and maximum constraints on age estimates for the biotic assemblages; e.g. the Avalon biotic assemblage may be at most 579 Ma and may persist in strata younger than 560 Ma.

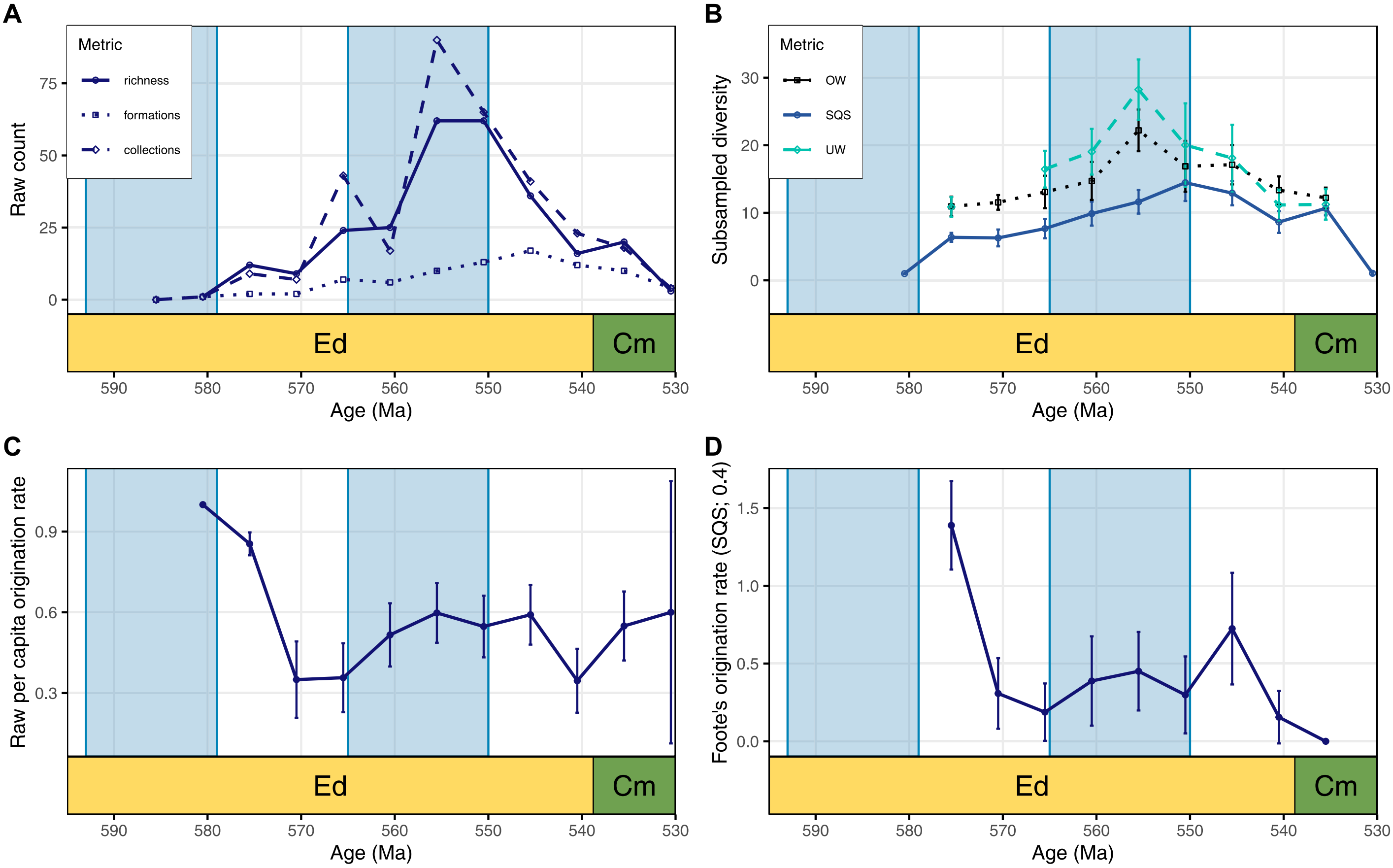

Figure 5. Paleobiodiversity metrics for the late Ediacaran biosphere. (A) Raw taxonomic richness (circles; solid lines) plotted alongside number of collections (diamonds; dashed lines) and number of formations (squares; dotted lines). (B) Subsampled taxonomic richness following shareholder quorum subsampling (SQS; quota = 0.4), unweighted collection-based classical rarefaction (UW; quota = 8 collections), and occurrence-weighted subsampling (OW; quota = 14 occurrences). (C) Raw per capita origination rate for 5 m.y. bins. (D) SQS (quota = 0.4) subsampled Foote's origination rate for 5 m.y. bins. The decline in values across the Ediacaran-Cambrian boundary is an artifact of our paleobiology data compilation, which focused on taxa with first occurrences in the Ediacaran Period. Error bars represent the standard deviations of 100 subsampling trials. Ed—Ediacaran (partial); Cm—Cambrian (partial). See also Supplemental Data S2, Table S9, and Figure S6 (text footnote 1).

589 Ma; Mills et al., 2017, 2024; Gómez et al., 2025, 2026). In particular, an ignimbrite interbedded with glaciogenic deposits of the Izdar Member, Morocco, yielded a radiometric date of 593.12 ± 0.14 Ma, which implies the onset of glacial conditions on West Gondwana by ca. 593 Ma (Letsch et al., 2018). The termination of the mid-Ediacaran icehouse is well constrained to ca. 579 Ma by radiometrically dated deposits in North Africa (Thomas et al., 2002; Inglis et al., 2004; Blein et al., 2014; Letsch et al., 2018; Youbi et al., 2020), the Rio de Plata craton (Oyhantçabal et al., 2007; Mallmann et al., 2007), and Avalonia (Pu et al., 2016). We do not envisage a static ice sheet lasting 15 m.y., but rather an ice sheet of uncertain but fluctuating dimensions, especially because of stratigraphic evidence for multiple advances and retreats of the ice line in the Tiddiline Group and Izdar Member deposits of West Gondwana (Letsch et al., 2018) and the Rocky Harbour Group deposits of Avalonia (Gómez et al., 2024, 2025, 2026).

Beyond the glaciogenic sedimentary record, circumstantial evidence also supports changes to climate state at ca. 600 Ma and ca. 579 Ma. In Oman, and elsewhere on the paleo-Gondwanan margin, the pre-Shuram CIE interval is characterized by condensed sedimentary successions, whereas there is a marked increase in depositional rates between ca. 580 Ma and ca. 560 Ma (Cantine et al., 2024). On the tropical-paleolatitude South China craton, stratigraphically constrained glendonite occurrences (indicative of cool- or cold-water conditions) in the Doushantuo Formation also indicate cooler ocean temperatures between ca. 600 Ma and ca. 579 Ma (Wang et al., 2017, 2020; Zhou et al., 2017), with an absence of glendonites after ca. 579 Ma and during the EN3/Shuram CIE (see the Supplemental Material).

The late Ediacaran icehouse is not as temporally well constrained as the mid-Ediacaran icehouse, and the age constraints of the late Ediacaran icehouse interval require testing by further radiometric dating. Most candidate glaciogenic deposits that we correlate to this interval are broadly bracketed by low-resolution radiometric dates or the Shuram CIE below and by latest Ediacaran or Cambrian fossils above (Fig. 2; Figs. S2 and S3). There are no deposits with well-constrained depositional ages during the Shuram CIE itself (ca. 574–567 Ma).

Indirect evidence from the broader geological record also lends support to a climate state transition before the terminal Ediacaran, likely at ca. 550 Ma. From a global rock record compilation, Bowyer et al. (2024) identified declining proportions of carbonate rocks and increasing proportions of silicate rocks by area and volume between ca. 565 Ma and ca. 550 Ma, culminating in a total absence of carbonate rocks ca. 555–550 Ma. There is a substantial hiatus in deposition on the South China craton between the uppermost Doushantuo Formation and the lowermost Dengying and Liuchapo Formations that is younger than EN3/Shuram CIE recovery (ca. 567 Ma) and older than 550.1 ± 0.6 Ma (Yang et al., 2021), coincident with Bowyer et al.'s (2024) potential global sea-level lowstand that reached a nadir ca. 550.5 Ma. The carbonate-barren ca. 555–550 Ma interval is followed by a marine transgression and increasing contribution of carbonates to the global rock record after ca. 550 Ma (Bowyer et al., 2024). Segessenman and Peters (2024) identified a contemporaneous approximately twofold increase in sediment volume flux across Laurentia from ca. 550.5 Ma and persisting until at least 545 Ma. The marine transgression (Bowyer et al., 2024) and increased sediment flux (Segessenman and Peters, 2024) may therefore reflect eustatic sea-level rise driven by melting land ice during the transition from the late Ediacaran icehouse to the terminal Ediacaran greenhouse, with associated increased weathering intensity and/or the flushing of glacial regolith into the oceans.

Above the ca. 550.5 Ma lowstand, the next identified global transgressive surface is at the Ediacaran-Cambrian boundary (Bowyer et al., 2024), arguably the best-known marine transgression in the stratigraphic record (Peters and Gaines, 2012), though of debated origin (e.g., Keller et al., 2018; Tasistro-Hart and Macdonald, 2023). In light of the emerging climate record through this interval, the lack of reported glaciogenic deposits of terminal Ediacaran (see "550–539 Ma: Terminal Ediacaran Greenhouse" section) or early Cambrian age (Boucot et al., 2013; Johnson et al., 2019; Wong Hearing et al., 2021; Álvaro et al., 2022) supports a tectono-eustatic rather than glacio-eustatic driver for this transgression (e.g., Tasistro-Hart and Macdonald, 2023).

What drove the changes in Ediacaran climate state is an open question. Shields et al. (2019) described how the oxidation of a large oceanic reservoir of dissolved organic carbon (DOC) could lead to elevated pCO_2 levels and global temperatures through the Shuram CIE, with a temperature-enhanced silicate-weathering feedback drawing down pCO_2 after the ocean DOC reservoir was exhausted. This temporally constrained mechanism would account for a Shuram interval greenhouse and post-Shuram cooling over several million years (Shields et al., 2019), as we infer from the Ediacaran glacial sedimentary record. Another potential driver of Ediacaran climate is the Central Iapetus magmatic province associated with breakup of Rodinia and the opening of the Iapetus Ocean (Youbi et al., 2020). Pulsed emplacement of large quantities of mafic igneous rock drives pCO_2 up from volcanic outgassing and then down via the silicate weathering feedback effect (Berner, 2004, 2006; Mills et al., 2019). Whatever the principal drivers of Ediacaran climate, our analysis provides a more tightly constrained framework for evaluating Earth system and biosphere evolution through this interval.

Coupling of Climate and Biosphere Dynamics

Our analysis suggests that step changes in the Ediacaran biosphere may have been coincident with changes in climate state at ca. 579 Ma, between ca. 565–560 Ma, and at ca. 550 Ma (Figs. 2, 4, and 5). Considering more proximate potential drivers of biotic change, Evans et al. (2022) found evidence for abiogenic influence, potentially oxygen availability, on Ediacaran biodiversity patterns, and Boag et al. (2024) related the ecophysiology of Ediacaran organisms to potential global temperature regimes, suggesting that high temperatures may have prevented the colonization of shallow-water settings during the Shuram CIE. Bowyer et al. (2024) linked Ediacaran biodiversity dynamics to long-term sea-level variation and potentially environmental oxygen availability. We suggest that first-order climate state changes could provide a first-order driving mechanism for the observed large-scale patterns in sea-level variation, oceanic oxygen availability, and ocean temperature, with the fossil record documenting the biosphere response.

Sea-level change has been implicated in shaping both apparent and real Ediacaran biodiversity dynamics by controlling available habitat space and the preserved rock record (Evans et al., 2022; Bowyer et al., 2024). In the Phanerozoic, marine transgressions and sea-level highstands, associated with warmer climate states, increased both shallow-marine habitat area and preservation potential of the shallow-marine shelf (Hallam and Wignall, 1999; Alroy, 2010b). Conversely, cooler intervals are associated with steeper latitudinal diversity gradients driven by increased thermal niche partitioning in the tropics, whereas warmer intervals are associated with flatter latitudinal diversity gradients and lower taxonomic richness (Song et al., 2020; Fenton et al., 2023; Woodhouse et al., 2023). Despite sampling limitations, it is notable that the highest Ediacaran taxonomic richness is found during an interval we interpret as the late Ediacaran icehouse (ca. 560–550 Ma; Fig. 5), characterized by low rock volume, a marine regression, and a sea-level lowstand (Bowyer et al., 2024). If this biodiversity signal is robust, our findings for the Ediacaran are similar to climatically driven diversity trends in the Phanerozoic (Song et al., 2020; Fenton et al., 2023; Woodhouse et al., 2023).

Ediacaran biosphere dynamics have been closely associated with ocean oxygenation as well as sea-level changes (Evans et al., 2018, 2022; Wood et al., 2019; Bowyer et al., 2024). Because an increase in temperature depresses oxygen solubility but elevates metabolic demand, the combination of temperature and ocean oxygenation is crucial for understanding marine habitability (Deutsch et al., 2015; Penn et al., 2018; Boag et al., 2018; Stockey et al., 2021). In this context, higher temperatures of the interpreted late Ediacaran greenhouse and terminal Ediacaran greenhouse intervals would have increased ecological stress by reducing thermal niche partitioning and oxygen availability. A resulting prediction is that generalist organisms with tolerance to low-oxygen conditions would fare better during icehouse to greenhouse transitions. Evans et al. (2022) found a positive correlation between organisms' surface area–to–volume ratio and survivorship through the White Sea to Nama transition and speculated that a high surface area–to–volume ratio would be beneficial to surviving in lower-oxygen environments. Our analysis suggests a possible mechanism for environmentally derived selectivity in the Ediacaran biosphere via global temperature change reflecting icehouse/greenhouse transitions.

We suggest that the ca. 565–560 Ma interval of global cooling at the beginning of the late Ediacaran icehouse made it possible for generalist taxonomic elements of the otherwise deep- and cold-water adapted Avalon biotic assemblage such as *Charnia* and *Charniodiscus* to colonize cooling shallow-marine environments (Boag et al., 2024). This is similar to the "polar emergence" pattern observed in the Antarctic fossil record during late Pliocene and early Pleistocene cooling episodes (Berkman et al., 2004), and it is the inverse of the present-day response to global heating (e.g., Perry et al., 2005). Cooling temperatures with associated increasing thermal gradients (Song et al., 2020; Fenton et al., 2023; Woodhouse et al., 2023), increasing oxygen availability, and decreasing metabolic oxygen demand (Deutsch et al., 2015; Penn et al., 2018; Boag et al., 2018; Stockey et al., 2021) at the beginning of the late Ediacaran icehouse may have increased niche availability across the greenhouse-to-icehouse transition, similar to the thermally driven polar diversity pump of the Cenozoic (Clarke and Crame, 1992; Griffiths et al., 2023).

Overall, the close correspondence between changes in Ediacaran paleobiology and paleoclimate supports the hypothesis of a close coupling between climate change and biosphere evolution established at least by the late Ediacaran Period. Notably, under our suggested climatic framework, the radiation of bilaterians appears to have occurred in shallower-water settings during a cold interval, and metazoan biomineralization and deep burrowing seem to have coincided with a transition from cold to warm conditions. We suggest that the coupling of biosphere and climate changes is evident despite uncertainties in global correlation and the known biases of both rock and fossil records (e.g., Bowyer et al., 2024), suggesting that it was a first-order property of the Ediacaran Earth system, as it is for the Phanerozoic.

CONCLUSIONS

Despite uncertainties in global correlation of Ediacaran strata, first-order transitions in late Ediacaran climate state appear to have been coincident with major turnovers in the biosphere (Fig. 4). Our analysis of candidate glaciogenic deposits suggests that Earth's climate during the mid- to late Ediacaran was characterized by two discrete intervals of icehouse conditions (mid-Ediacaran icehouse: ca. 593–579 Ma, and late Ediacaran icehouse: ca. 565–550 Ma) and two discrete intervals of greenhouse conditions (late Ediacaran greenhouse: ca. 579–565 Ma, and terminal Ediacaran greenhouse: ca. 550 Ma into the early Cambrian; Fig. 2). Furthermore, there is no robust evidence for icehouse climate conditions in the terminal Ediacaran immediately preceding the Phanerozoic Eon. There is wide scope for further work in this area: The causal mechanisms of Ediacaran climatic changes require greater investigation; the known Ediacaran fossil record is particularly unevenly sampled; and the glacial record requires work to constrain both the depositional ages and potential glaciogenicity of many of its deposits. In particular, deposits associated with the late Ediacaran icehouse are not as well constrained by radiometric ages as are those associated with the mid-Ediacaran icehouse (though not for lack of effort; e.g., Wu et al., 2024a). Increasing the coverage of radiometric dates for late Ediacaran icehouse–associated deposits should be a priority for future research and would provide a test of the climatic framework proposed herein. We encourage rigorous testing of the climatic and biotic framework we propose here, which from the currently available evidence supports a Phanerozoic-style coupling of metazoan evolution and climate change since the Ediacaran Period.

ACKNOWLEDGMENTS

We gratefully acknowledge funding from The Leverhulme Trust, grant RPG-2022-233 to M. Williams, T.H.P. Harvey, A.G. Liu, and A. Pohl (Earth System Dynamics at the Dawn of the Animal-Rich Biosphere), and the Natural Environment Research Council (NERC) Cambridge Climate, Life and Earth (C-CLEAR) Doctoral Training Partnership (supporting the Ph.D. studentship of B.H. Tindal). We are grateful to Graham Shields, Georgina Virgo, Carol Dehler, and other anonymous reviewers, whose comments greatly improved previous versions of this manuscript.

REFERENCES CITED

Agić, H., Jensen, S., Meinhold, G., Högström, A.E.S., Ebbestad, J.O.R., Høyberget, M., Palacios, T., and Taylor, W.L., 2024, Life through an Ediacaran glaciation: Shale- and diamictite-hosted organic-walled microfossil assemblages from the late Neoproterozoic of the Tanafjorden area, northern Norway: Palaeogeography, Palaeoclimatology, Palaeoecology, v. 635, https://doi.org/10.1016/j.palaeo.2023.111956.

Alexeiev, D.V., Khudoley, A.K., Shevkunov, A.G., Kulikova, A.V., Aidarkulov, T.N., and Minnebaev, K.R., 2025, Late Ediacaran glacial deposits of the Baykonur Formation, Middle Tianshan of east Kyrgyzstan: Age substantiation based on detrital zircon U-Th-Pb (LA-ICP-MS) geochronological study: Doklady Earth Sciences, v. 520, p. 24, https://doi.org/10.1134/S1028334X24604838.

Alroy, J., 2010a, Fair sampling of taxonomic richness and unbiased estimation of origination and extinction rates: The Paleontological Society Papers, v. 16, p. 55–80, https://doi.org/10.1017/S1089332600001819.

Alroy, J., 2010b, Geographical, environmental and intrinsic biotic controls on Phanerozoic marine diversification: Palaeontology, v. 53, p. 1211–1235, https://doi.org/10.1111/j.1475-4983.2010.01011.x.

Alroy, J., 2014, Accurate and precise estimates of origination and extinction rates: Paleobiology, v. 40, p. 374–397, https://doi.org/10.1666/13036.

Álvaro, J.J., Cortijo, I., Jensen, S., Lorenzo, S., and Pieren, A.P., 2019, Updated stratigraphic framework and biota of the Ediacaran and Terreneuvian in the Alcudia-Toledo Mountains of the Central Iberian zone, Spain: Estudios Geológicos, v. 75, https://doi.org/10.3989/egeol.43620.548.

Álvaro, J.J., Johnson, S.C., Barr, S.M., Jensen, S., Palacios, T., van Rooyen, D., and White, C.E., 2022, Unconformity-bounded rift sequences in Terreneuvian–Miaolingian strata of the Caledonian Highlands, Atlantic Canada: Geological Society of America Bulletin, v. 135, p. 1225–1242, https://doi.org/10.1130/B36402.1.

Amorim, K.B., Afonso, J.W.L., Leme, J.M., Diniz, C.Q.C., Rivera, L.C.M., Gómez-Gutiérrez, J.C., Boggiani, P.C., and Trindade, R.I.F., 2020, Sedimentary facies, fossil distribution and depositional setting of the late Ediacaran Tamengo Formation (Brazil): Sedimentology, v. 67, p. 3422–3450, https://doi.org/10.1111/sed.12749.

Anderson, M.M., 1972, A possible time span for the late Precambrian of the Avalon Peninsula, southeastern Newfoundland, in the light of worldwide correlation of fossils, tillites, and rock units within the succession: Canadian Journal of Earth Sciences, v. 9, p. 1710–1726, https://doi.org/10.1139/e72-151.

Arnaud, E., Halverson, G.P., and Shields-Zhou, G., eds., 2011, The Geological Record of Neoproterozoic Glaciations: Geological Society, London, Memoir 36, 735 p., https://doi.org/10.1144/M36.

Baillie, I.M., Nelson, L., Almond, J., Swart, R., Penn-Clarke, C., Polomski, D., Helms, L., Cardy, J., Bezuidenhout, K., and Smith, E., 2025, No late Ediacaran glaciation recorded in the Nama Group, *in* Goldschmidt Conference 2025: https://conf.goldschmidt.info/goldschmidt/2025/meetingapp.cgi/Paper/30215.

Bennett, M.R., Doyle, P., and Mather, A.E., 1996, Dropstones: Their origin and significance: Palaeogeography, Palaeoclimatology, Palaeoecology, v. 121, p. 331–339, https://doi.org/10.1016/0031-0182(95)00071-2.

Bergmann, K., Osburn, M.R., Wilcots, J., Cantine, M., Grotzinger, J.P., Fischer, W.W., Eiler, J.M., and Bonifacie, M., 2022, The Shuram excursion: A response to climate extremes at the dawn of animal life: ESS Open Archive, 15 July 2022, https://doi.org/10.1002/essoar.10511917.1.

Berkman, P.A., Cattaneo-Vietti, R., Chiantore, M., and Howard-Williams, C., 2004, Polar emergence and the influence of increased sea-ice extent on the Cenozoic biogeography of pectinid molluscs in Antarctic coastal areas: Deep-Sea Research Part II: Topical Studies in Oceanography, v. 51, p. 1839–1855, https://doi.org/10.1016/j.dsr2.2004.07.017.

Berner, R.A., 2004, The Phanerozoic Carbon Cycle: CO_2 and O_2: New York, Oxford University Press, 159 p., https://doi.org/10.1093/oso/9780195173338.001.0001.

Berner, R.A., 2006, Inclusion of the weathering of volcanic rocks in the GEOCARBSULF Model: American Journal of Science, v. 306, p. 295–302, https://doi.org/10.2475/05.2006.01.

Betts, M.J., et al., 2018, Early Cambrian chronostratigraphy and geochronology of South Australia: Earth-Science Reviews, v. 185, p. 498–543, https://doi.org/10.1016/j.earscirev.2018.06.005.

Blein, O., et al., 2014, Geochronological constraints on the polycyclic magmatism in the Bou Azzer–El Graara inlier (central Anti-Atlas Morocco): Journal of African Earth Sciences, v. 99, p. 287–306, https://doi.org/10.1016/j.jafrearsci.2014.04.021.

Boag, T.H., Darroch, S.A.F., and Laflamme, M., 2016, Ediacaran distributions in space and time: Testing assemblage concepts of earliest macroscopic body fossils: Paleobiology, v. 42, p. 574–594, https://doi.org/10.1017/pab.2016.20.

Boag, T.H., Stockey, R.G., Elder, L.E., Hull, P.M., and Sperling, E.A., 2018, Oxygen, temperature and the deep-marine stenothermal cradle of Ediacaran evolution: Proceedings of the Royal Society B: Biological Sciences, v. 285, https://doi.org/10.1098/rspb.2018.1724.

Boag, T.H., Busch, J.F., Gooley, J.T., Strauss, J.V., and Sperling, E.A., 2024, Deep-water first occurrences of Ediacara biota prior to the Shuram carbon isotope excursion in the Wernecke Mountains, Yukon, Canada: Geobiology, v. 22, https://doi.org/10.1111/gbi.12597.

Boddy, C.E., Mitchell, E.G., Merdith, A., and Liu, A.G., 2021, Palaeolatitudinal distribution of the Ediacaran macrobiota: Journal of the Geological Society, v. 179, https://doi.org/10.1144/jgs2021-030.

Bond, D.P.G., and Grasby, S.E., 2017, On the causes of mass extinctions: Palaeogeography, Palaeoclimatology, Palaeoecology, v. 478, p. 3–29, https://doi.org/10.1016/j.palaeo.2016.11.005.

Bossi, J., Cingolani, C.A., Llambías, E.J., Varela, R., and Campal, N., 1993, Características del magmatismo post-orogénico finibrasiliano en el Uruguay: Formaciones Sierra de Ríos y Sierra de Ánimas: Brazilian Journal of Geology, v. 23, no. 3, p. 282–288.

Boucot, A.J., Xu, C., Scotese, C.R., and Morley, R.J., 2013, Phanerozoic Paleoclimate: An Atlas of Lithologic Indicators of Climate: SEPM (Society for Sedimentary Geology) Concepts in Sedimentology and Paleontology 11, 478 p., https://doi.org/10.2110/sepmcsp.11.

Bowring, S.A., Grotzinger, J.P., Condon, D.J., Ramezani, J., Newall, M.J., and Allen, P.A., 2007, Geochronologic constraints on the chronostratigraphic framework of the Neoproterozoic Huqf Supergroup, Sultanate of Oman: American Journal of Science, v. 307, p. 1097–1145, https://doi.org/10.2475/10.2007.01.

Bowyer, F.T., Zhuravlev, A.Y., Wood, R., Shields, G.A., Zhou, Y., Curtis, A., Poulton, S.W., Condon, D.J., Yang, C., and Zhu, M., 2022, Calibrating the temporal and spatial dynamics of the Ediacaran–Cambrian radiation of animals: Earth-Science Reviews, v. 225, https://doi.org/10.1016/j.earscirev.2021.103913.

Bowyer, F.T., Uahengo, C.-I., Kaputuaza, K., Ndeunyema, J., Yilales, M., Alexander, R.D., Curtis, A., and Wood, R.A., 2023, Constraining the onset and environmental setting of metazoan biomineralization: The Ediacaran Nama Group of the Tsaus Mountains, Namibia: Earth and Planetary Science Letters, v. 620, https://doi.org/10.1016/j.epsl.2023.118336.

Bowyer, F.T., Wood, R.A., and Yilales, M., 2024, Sea level controls on Ediacaran–Cambrian animal radiations: Science Advances, v. 10, https://doi.org/10.1126/sciadv.ado6462.

Brückner, D., and Anderson, M.M., 1971, Late Precambrian glacial deposits in southeastern Newfoundland—A preliminary note: Geological Association of Canada Proceedings, v. 24, p. 95–102.

Burns, S., and Matter, A., 1993, Carbon isotopic record of latest Proterozoic from Oman: Eclogae Geologicae Helvetiae, v. 86, p. 595–607.

Busch, J.F., Hodgin, E.B., Ahm, A.-S.C., Husson, J.M., Macdonald, F.A., Bergmann, K.D., Higgins, J.A., and Strauss, J.V., 2022, Global and local drivers of the Ediacaran Shuram carbon isotope excursion: Earth and Planetary Science Letters, v. 579, https://doi.org/10.1016/j.epsl.2022.117368.

Busch, J.F., Boag, T.H., Sperling, E.A., Rooney, A.D., Feng, X., Moynihan, D.P., and Strauss, J.V., 2023, Integrated litho-, chemo- and sequence stratigraphy of the Ediacaran Gametrail Formation across a shelf-slope transect in the Wernecke Mountains, Yukon, Canada: American Journal of Science, v. 323, 4, https://doi.org/10.2475/001c.74874.

Butterfield, N.J., 2009, Macroevolutionary turnover through the Ediacaran transition: Ecological and biogeochemical implications, *in* Craig, J., Thurow, J., Thusu, B., Whitham, A., and Abutarruma, Y., eds., Global Neoproterozoic Petroleum Systems: The Emerging Potential in North Africa: Geological Society, London, Special Publication 326, p. 55–66, https://doi.org/10.1144/SP326.3.

Cantine, M.D., Rooney, A.D., Knoll, A.H., Gómez-Pérez, I., Al Baloushi, B., and Bergmann, K.D., 2024, Chronology of Ediacaran sedimentary and biogeochemical shifts along eastern Gondwanan margins: Communications Earth & Environment, v. 5, 520, https://doi.org/10.1038/s43247-024-01630-1.

Carbone, C.A., Narbonne, G.M., Macdonald, F.A., and Boag, T.H., 2015, New Ediacaran fossils from the uppermost Blueflower Formation, northwest Canada: Disentangling biostratigraphy and paleoecology: Journal of Paleontology, v. 89, p. 281–291, https://doi.org/10.1017/jpa.2014.25.

Carto, S.L., and Eyles, N., 2011, The deep-marine glaciogenic Gaskiers Formation, Newfoundland, Canada, *in* Arnaud, E., Halverson, G.P., and Shields-Zhou, G., eds., The Geological Record of Neoproterozoic Glaciations: Geological Society, London, Memoir 36, p. 467–473, https://doi.org/10.1144/M36.42.

Carto, S.L., and Eyles, N., 2012, Sedimentology of the Neoproterozoic (c. 580 Ma) Squantum 'Tillite,' Boston Basin, USA: Mass flow deposition in a deep-water arc basin lacking direct glacial influence: Sedimentary Geology, v. 269–270, p. 1–14, https://doi.org/10.1016/j.sedgeo.2012.03.011.

Chumakov, N.M., 2007, Climates and climate zonality of the Vendian: Geological evidence, *in* Vickers-Rich, P., and Komarower, P., eds., The Rise and Fall of the Ediacaran Biota: Geological Society, London, Special Publication 286, p. 15–26, https://doi.org/10.1144/SP286.2.

Chumakov, N.M., 2009, The Baykonurian glaciohorizon of the late Vendian: Stratigraphy and Geological Correlation, v. 17, p. 373–381, https://doi.org/10.1134/S0869593809040029.

Chumakov, N.M., 2011a, The Neoproterozoic glacial formations of the North and Middle Urals, *in* Arnaud, E., Halverson, G.P., and Shields-Zhou, G., eds., The Geological Record of Neoproterozoic Glaciations: Geological Society, London, Memoir 36, p. 289–296, https://doi.org/10.1144/M36.24.

Chumakov, N.M., 2011b, Glacial deposits of the Baykonur Formation, Kazakhstan and Kyrgyzstan, *in* Arnaud, E., Halverson, G.P., and Shields-Zhou, G., eds., The Geological Record of Neoproterozoic Glaciations: Geological Society, London, Memoir 36, p. 303–307, https://doi.org/10.1144/M36.26.

Chumakov, N.M., Pokrovskii, B.G., and Maslov, A.V., 2013, Stratigraphic position and significance of carbonate rocks related to Neoproterozoic glacial horizons of the Urals: Stratigraphy and Geological Correlation, v. 21, p. 573–591, https://doi.org/10.1134/S0869593813060038.

Clarke, A., and Crame, J.A., 1992, The Southern Ocean benthic fauna and climate change: A historical perspective: Philosophical Transactions of the Royal Society of London B: Biological Sciences, v. 338, p. 299–309, https://doi.org/10.1098/rstb.1992.0150.

Clarke, A.J.I., Kirkland, C.L., Menon, L.R., Condon, D.J., Cope, J.C.W., Bevins, R.E., and Glorie, S., 2024, U-Pb zircon-rutile dating of the Llangynog Inlier, Wales: Constraints on an Ediacaran shallow-marine fossil assemblage from East Avalonia: Journal of the Geological Society, v. 181, https://doi.org/10.1144/jgs2023-081.

Cohen, K.M., Harper, D.A.T., and Gibbard, P.L., 2013, The ICS International Chronostratigraphic Chart: Episodes, v. 36, p. 199–204, https://doi.org/10.18814/epiiugs/2013/v36i3/002.

Cope, J.C.W., 1977, An Ediacara-type fauna from South Wales: Nature, v. 268, 624, https://doi.org/10.1038/268624a0.

Cope, J.C.W., 1983, Precambrian faunas from the Carmarthen district: Nature in Wales, v. 1, p. 11–16, https://journals.library.wales/view/1220475/1224653/13#?m=69&xywh=-3724%2C0%2C10423%2C3974&cv=12.

Darroch, S.A.F., et al., 2015, Biotic replacement and mass extinction of the Ediacara biota: Proceedings of the Royal Society B: Biological Sciences, v. 282, https://doi.org/10.1098/rspb.2015.1003.

Deutsch, C., Ferrel, A., Seibel, B., Pörtner, H.-O., and Huey, R.B., 2015, Climate change tightens a metabolic constraint on marine habitats: Science, v. 348, p. 1132–1135, https://doi.org/10.1126/science.aaa1605.

Dott, R.H., Jr., 1961, Squantum "tillite", Massachusetts—Evidence of glaciation or subaqueous mass movements?: Geological Society of America Bulletin, v. 72, p. 1289–1305, https://doi.org/10.1130/0016-7606(1961)72[1289:STMOGO]2.0.CO;2.

Dunn, F.S., Kenchington, C.G., Parry, L.A., Clark, J.W., Kendall, R.S., and Wilby, P.R., 2022, A crown-group cnidarian from the Ediacaran of Charnwood Forest, UK: Nature Ecology & Evolution, v. 6, p. 1095–1104, https://doi.org/10.1038/s41559-022-01807-x.

Erwin, D.H., 2009, Climate as a driver of evolutionary change: Current Biology, v. 19, p. R575–R583, https://doi.org/10.1016/j.cub.2009.05.047.

Etemad-Saeed, N., Hosseini-Barzi, M., Adabi, M.H., Miller, N.R., Sadeghi, A., Houshmandzadeh, A., and Stockli, D.F., 2016, Evidence for ca. 560 Ma Ediacaran glaciation in the Kahar Formation, central Alborz Mountains, northern Iran: Gondwana Research, v. 31, p. 164–183, https://doi.org/10.1016/j.gr.2015.01.005.

Evans, S.D., Diamond, C.W., Droser, M.L., and Lyons, T.W., 2018, Dynamic oxygen and coupled biological and ecological innovation during the second wave of the Ediacara Biota: Emerging Topics in Life Sciences, v. 2, p. 223–233, https://doi.org/10.1042/ETLS20170148.

Evans, S.D., Tu, C., Rizzo, A., Surprenant, R.L., Boan, P.C., McCandless, H., Marshall, N., Xiao, S., and Droser, M.L., 2022, Environmental drivers of the first major animal extinction across the Ediacaran White Sea–Nama transition: Proceedings of the National Academy of Sciences of the United States of America, v. 119, https://doi.org/10.1073/pnas.2207475119.

Eyles, N., Eyles, C.H., and Miall, A.D., 1983, Lithofacies types and vertical profile models: An alternative approach to the description and environmental interpretation of glacial diamict and diamictite sequences: Sedimentology, v. 30, p. 393–410, https://doi.org/10.1111/j.1365-3091.1983.tb00679.x.

Fedonkin, M.A., Vickers-Rich, P., Swalla, B.J., Trusler, P., and Hall, M., 2012, A new metazoan from the Vendian of the White Sea, Russia, with possible affinities to the ascidians: Paleontological Journal, v. 46, p. 1–11, https://doi.org/10.1134/S0031030112010042.

Fenton, I.S., Aze, T., Farnsworth, A., Valdes, P., and Saupe, E.E., 2023, Origination of the modern-style diversity gradient 15 million years ago: Nature, v. 614, p. 708–712, https://doi.org/10.1038/s41586-023-05712-6.

Fischer, A.G., 1981, Climatic oscillations in the biosphere, *in* Nitecki, M.H., ed., Biotic Crises in Ecological and Evolutionary Time: San Diego, California, Academic Press, p. 103–131, https://doi.org/10.1016/B978-0-12-519640-6.50012-0.

Fischer, A.G., 1982, Long-term climatic oscillations recorded in stratigraphy, *in* Berger, W., ed., Climate in Earth History: Washington, D.C., National Academy Press, National Research Council, Studies in Geophysics, p. 97–104, https://doi.org/10.17226/11798.

Fitzgerald, D.M., Narbonne, G.M., Pufahl, P.K., and Dalrymple, R.W., 2024, The Mall Bay Formation (Ediacaran) and the protracted onset of the Gaskiers glaciation in Newfoundland, Canada: Precambrian Research, v. 405, https://doi.org/10.1016/j.precamres.2024.107369.

Flint, R.F., Sanders, J.E., and Rodgers, J., 1960a, Diamictite, a substitute term for symmictite: Geological Society of America Bulletin, v. 71, p. 1809–1810, https://doi.org/10.1130/0016-7606(1960)71[1809:DASTFS]2.0.CO;2.

Flint, R.F., Sanders, J.E., and Rodgers, J., 1960b, Symmictite: A name for nonsorted terrigenous sedimentary rocks that contain a wide range of particle sizes: Geological Society of America Bulletin, v. 71, p. 507–510, https://doi.org/10.1130/0016-7606(1960)71[507:SANFNT]2.0.CO;2.

Frakes, L.A., Francis, J.E., and Syktus, J.I., 1992, Climate Modes of the Phanerozoic: Cambridge, UK, Cambridge University Press, 274 p., https://doi.org/10.1017/CBO9780511628948.

Francovschi, I., Shumlyanskyy, L., Grytsenko, V., Hoffmann, A., Wilde, S.A., and Bekker, A., 2024, U-Pb geochronology and Hf isotope systematics of detrital zircon from the basal part of the late Ediacaran sedimentary succession of the Moldova-Podillya basin (SW Baltica): Implications for glacial vs. alluvial origin: Precambrian Research, v. 413, https://doi.org/10.1016/j.precamres.2024.107572.

Gaucher, C., Blanco, G., Chiglino, L., Poiré, D., and Germs, G.J.B., 2008, Acritarchs of Las Ventanas Formation (Ediacaran, Uruguay): Implications for the timing of coeval rifting and glacial events in western Gondwana: Gondwana Research, v. 13, p. 488–501, https://doi.org/10.1016/j.gr.2007.05.008.

Gearty, W., 2026, deeptime: An R package that facilitates highly customizable and reproducible visualizations of data over geological time intervals: Big Earth Data, v. 10, no. 1, p. 1–17, https://doi.org/10.1080/20964471.2025.2537516.

Gehling, J.G., and Droser, M.L., 2013, How well do fossil assemblages of the Ediacara Biota tell time?: Geology, v. 41, p. 447–450, https://doi.org/10.1130/G33881.1.

Gehling, J.G., and Narbonne, G.M., 2007, Spindle-shaped Ediacara fossils from the Mistaken Point assemblage, Avalon zone, Newfoundland: Canadian Journal of Earth Sciences, v. 44, p. 367–387, https://doi.org/10.1139/e07-003.

Gehling, J.G., Narbonne, G.M., and Anderson, M.M., 2000, The first named Ediacaran body fossil, *Aspidella terranovica*: Palaeontology, v. 43, p. 427–456, https://doi.org/10.1111/j.0031-0239.2000.00134.x.

Germs, G.J.B., and Gaucher, C., 2012, Nature and extent of a late Ediacaran (ca. 547 Ma) glacigenic erosion surface in southern Africa: South African Journal of Geology, v. 115, p. 91–102, https://doi.org/10.2113/gssajg.115.91.

Gómez, N., Lowe, D., Mills, A., Slaney, N., and Arnott, B., 2024, Ediacaran proximal glaciomarine sedimentation in the Bonavista Peninsula, Avalon zone (Newfoundland), *in* Proceedings of the European Geosciences Union General Assembly 2024: Vienna, Austria, European Geosciences Union, https://doi.org/10.5194/egusphere-egu24-6919.

Gómez, N., Lowe, D., Kommescher, S., and Mills, A., 2025, Unraveling recycling and climate influence on detrital U-Pb geochronology of titanite and apatite: An example from the Gaskiers glaciation in Newfoundland: Precambrian Research, v. 427, https://doi.org/10.1016/j.precamres.2025.107871.

Gómez, N., Lowe, D., Mills, A., Kommescher, S., and Lam, R., 2026, Interplay of Ediacaran glaciation and sediment provenance revealed by detrital zircon U-Pb geochronology and Hf isotope geochemistry in the Bonavista Peninsula (Newfoundland): Geological Society of America Bulletin, v. 138, p. 279–298, https://doi.org/10.1130/B38347.1.

Grazhdankin, D., 2004, Patterns of distribution in the Ediacaran biotas: Facies versus biogeography and evolution:

Paleobiology, v. 30, p. 203–221, https://doi.org/10.1666/0094-8373(2004)030<0203:PODITE>2.0.CO;2.
Grazhdankin, D., 2014, Patterns of evolution of the Ediacaran soft-bodied biota: Journal of Paleontology, v. 88, p. 269–283, https://doi.org/10.1666/13-072.
Grazhdankin, D.V., Maslov, A.V., and Krupenin, M.T., 2009, Structure and depositional history of the Vendian Sylvitsa Group in the western flank of the Central Urals: Stratigraphy and Geological Correlation, v. 17, p. 476–492, https://doi.org/10.1134/S0869593809050025.
Grazhdankin, D.V., Marusin, V.V., Meert, J., Krupenin, M.T., and Maslov, A.V., 2011, Kotlin regional stage in the South Urals: Doklady Earth Sciences, v. 440, p. 1222–1226, https://doi.org/10.1134/S1028334X11090170.
Griffiths, H.J., Whittle, R.J., and Mitchell, E.G., 2023, Animal survival strategies in Neoproterozoic ice worlds: Global Change Biology, v. 29, p. 10–20, https://doi.org/10.1111/gcb.16393.
Hallam, A., and Wignall, P.B., 1999, Mass extinctions and sea-level changes: Earth-Science Reviews, v. 48, p. 217–250, https://doi.org/10.1016/S0012-8252(99)00055-0.
Halverson, G.P., Hoffman, P.F., Schrag, D.P., Maloof, A.C., and Rice, A.H.N., 2005, Toward a Neoproterozoic composite carbon-isotope record: Geological Society of America Bulletin, v. 117, p. 1181–1207, https://doi.org/10.1130/B25630.1.
Hambrey, M.J., and Glasser, N.F., 2003, Glacial sediments: Processes, environments and facies, *in* Middleton, G.V., Church, M.J., Coniglio, M., Hardie, L.A., and Longstaffe, F.J., eds., Encyclopedia of Sediments and Sedimentary Rocks: Dordrecht, Netherlands, Springer, p. 316–331, https://doi.org/10.1007/978-1-4020-3609-5_99.
Hambrey, M.J., and Harland, W.B., 1981a, Criteria for the identification of glacigenic deposits, *in* Hambrey, M.J., and Harland, W.B., eds., Earth's Pre-Pleistocene Glacial Record: Cambridge, UK, Cambridge University Press, p. 14–21.
Hambrey, M.J., and Harland, W.B., eds., 1981b, Earth's Pre-Pleistocene Glacial Record: Cambridge, UK, Cambridge University Press, 1004 p.
Hawco, J.B., Kenchington, C.G., and McIlroy, D., 2021, A quantitative and statistical discrimination of morphotaxa within the Ediacaran genus *Palaeopascichnus*: Papers in Palaeontology, v. 7, p. 657–673, https://doi.org/10.1002/spp2.1290.
Hoffman, P.F., et al., 2017, Snowball Earth climate dynamics and Cryogenian geology-geobiology: Science Advances, v. 3, https://doi.org/10.1126/sciadv.1600983.
Hofmann, H.J., Fritz, W.H., and Narbonne, G.M., 1983, Ediacaran (Precambrian) fossils from the Wernecke Mountains, northwestern Canada: Science, v. 221, p. 455–457, https://doi.org/10.1126/science.221.4609.455.
Hofmann, H.J., O'Brien, S.J., and King, A.F., 2008, Ediacaran Biota on Bonavista Peninsula, Newfoundland, Canada: Journal of Paleontology, v. 82, p. 1–36, https://doi.org/10.1666/06-087.1.
Högström, A., Jensen, S., Palacios, T., and Ebbestad, J.O.R., 2013, New information on the Ediacaran-Cambrian transition in the Vestertana Group, Finnmark, northern Norway, from trace fossils and organic-walled microfossils: Norsk Geologisk Tidsskrift, v. 93, p. 95–106.
Hu, W., and McSaveney, M.J., 2018, A polished and striated pavement formed by a rock avalanche in under 90 s mimics a glacially striated pavement: Geomorphology, v. 320, p. 154–161, https://doi.org/10.1016/j.geomorph.2018.08.011.
Inglis, J.D., MacLean, J.S., Samson, S.D., D'Lemos, R.S., Admou, H., and Hefferan, K., 2004, A precise U-Pb zircon age for the Bleïda granodiorite, Anti-Atlas, Morocco: Implications for the timing of deformation and terrane assembly in the eastern Anti-Atlas: Journal of African Earth Sciences, v. 39, p. 277–283, https://doi.org/10.1016/j.jafrearsci.2004.07.041.
Jensen, S., Högström, A.E.S., Høyberget, M., Meinhold, G., McIlroy, D., Ebbestad, J.O.R., Taylor, W.L., Agić, H., and Palacios, T., 2018, New occurrences of *Palaeopascichnus* from the Stáhpogieddi Formation, Arctic Norway, and their bearing on the age of the Varanger Ice Age: Canadian Journal of Earth Sciences, v. 55, p. 1253–1261, https://doi.org/10.1139/cjes-2018-0035.
Johnson, S., McLeod, M., and Branscombe, L., 2019, A note on the location of diamictite in the Ratcliffe Brook Group on Hanford Brook, southern New Brunswick, Canada, *in* 45th Atlantic Geoscience Society (AGS) Colloquium and Annual Meeting: Fredericton, New Brunswick, Canada: The Atlantic Geoscience Society (La Société Géoscientifique de l'Atlantique), p. 35–36, https://atlanticgeosciencesociety.ca/wp-content/uploads/2021/02/program_and_abstracts_2019.pdf.
Judd, E.J., Tierney, J.E., Lunt, D.J., Montañez, I.P., Huber, B.T., Wing, S.L., and Valdes, P.J., 2024, A 485-million-year history of Earth's surface temperature: Science, v. 385, https://doi.org/10.1126/science.adk3705.
Keller, C.B., Husson, J.M., Mitchell, R.N., Bottke, W.F., Gernon, T.M., Boehnke, P., Bell, E.A., Swanson-Hysell, N.L., and Peters, S.E., 2018, Neoproterozoic glacial origin of the Great Unconformity: Proceedings of the National Academy of Sciences of the United States of America, v. 116, p. 1136–1145, https://doi.org/10.1073/pnas.1804350116.
Kenchington, C.G., Harris, S.J., Vixseboxse, P.B., Pickup, C., and Wilby, P.R., 2018, The Ediacaran fossils of Charnwood Forest: Shining new light on a major biological revolution: Proceedings of the Geologists' Association, v. 129, p. 264–277, https://doi.org/10.1016/j.pgeola.2018.02.006.
Kennedy, K., and Eyles, N., 2021, Syn-rift mass flow generated 'tectonofacies' and 'tectonosequences' of the Kingston Peak Formation, Death Valley, California, and their bearing on supposed Neoproterozoic panglacial climates: Sedimentology, v. 68, p. 352–381, https://doi.org/10.1111/sed.12781.
Kennedy, K., Eyles, N., and Broughton, D., 2019, Basinal setting and origin of thick (1·8 km) mass-flow dominated Grand Conglomérat diamictites, Kamoa, Democratic Republic of Congo: Resolving climate and tectonic controls during Neoproterozoic glaciations: Sedimentology, v. 66, p. 556–589, https://doi.org/10.1111/sed.12494.
Kidder, D.L., and Worsley, T.R., 2010, Phanerozoic large igneous provinces (LIPs), HEATT (haline euxinic acidic thermal transgression) episodes, and mass extinctions: Palaeogeography, Palaeoclimatology, Palaeoecology, v. 295, p. 162–191, https://doi.org/10.1016/j.palaeo.2010.05.036.
Kocsis, Á.T., Reddin, C.J., Alroy, J., and Kiessling, W., 2019, The r package divDyn for quantifying diversity dynamics using fossil sampling data: Methods in Ecology and Evolution, v. 10, p. 735–743, https://doi.org/10.1111/2041-210X.13161.
Kröner, A., 1981, A29. Late Precambrian diamictites of South Africa and Namibia, *in* Hambrey, M.J., and Harland, W.B., eds., Earth's Pre-Pleistocene Glacial Record: Cambridge, UK, Cambridge University Press, p. 167–177, https://unesdoc.unesco.org/ark:/48223/pf0000141486.
Kröner, A., and Germs, G.J.B., 1971, A re-interpretation of the Numees-Nama contact at Aussenkjer, southwest Africa: Transactions of the Geological Society of South Africa, v. 74, p. 69–74.
Kühnemann, V., Meinhold, G., Schulz, B., Gilbricht, S., Weber, S., and Wemmer, K., 2025, The "greywacke problem" explored in the Neoproterozoic of Saxo-Thuringia: New insights into sediment composition and metamorphic overprint: International Journal of Earth Sciences, v. 114, p. 23–54, https://doi.org/10.1007/s00531-024-02475-x.
Le Heron, D.P., Vandyk, T.M., Kuang, H., Liu, Y., Chen, X., Wang, Y., Yang, Z., Scharfenberg, L., Davies, B., and Shields, G., 2019, Bird's-eye view of an Ediacaran subglacial landscape: Geology, v. 47, p. 705–709, https://doi.org/10.1130/G46285.1.
Letsch, D., Large, S.J.E., Buechi, M.W., Winkler, W., and von Quadt, A., 2018, Ediacaran glaciations of the West African craton—Evidence from Morocco: Precambrian Research, v. 310, p. 17–38, https://doi.org/10.1016/j.precamres.2018.02.015.
Linnemann, U., et al., 2018, A ∼565 Ma old glaciation in the Ediacaran of peri-Gondwanan West Africa: International Journal of Earth Sciences, v. 107, p. 885–911, https://doi.org/10.1007/s00531-017-1520-7.
Linnemann, U., et al., 2019, New high-resolution age data from the Ediacaran-Cambrian boundary indicate rapid, ecologically driven onset of the Cambrian explosion: Terra Nova, v. 31, p. 49–58, https://doi.org/10.1111/ter.12368.
Linnemann, U., et al., 2022, An Upper Ediacaran glacial period in Cadomia: The Granville tillite (Armorican Massif)—Sedimentology, geochronology and provenance: Geological Magazine, v. 159, p. 999–1013, https://doi.org/10.1017/S0016756821001011.
Liu, A.G., 2011, Reviewing the Ediacaran fossils of the Long Mynd, Shropshire: Proceedings of the Shropshire Geological Society, v. 16, p. 31–43.
Liu, A.G., McIlroy, D., and Brasier, M.D., 2010, First evidence for locomotion in the Ediacara biota from the 565 Ma Mistaken Point Formation, Newfoundland: Geology, v. 38, p. 123–126, https://doi.org/10.1130/G30368.1.
Liu, A.G., Matthews, J.J., Menon, L.R., McIlroy, D., and Brasier, M.D., 2014a, *Haootia quadriformis* n. gen., n. sp., interpreted as a muscular cnidarian impression from the late Ediacaran period (approx. 560 Ma): Proceedings of the Royal Society B: Biological Sciences, v. 281, https://doi.org/10.1098/rspb.2014.1202.
Liu, A.G., McIlroy, D., Matthews, J.J., and Brasier, M.D., 2014b, Confirming the metazoan character of a 565 Ma trace-fossil assemblage from Mistaken Point, Newfoundland: PALAIOS, v. 29, p. 420–430, https://doi.org/10.2110/palo.2014.011.
Liu, A.G., Kenchington, C.G., and Mitchell, E.G., 2015, Remarkable insights into the paleoecology of the Avalonian Ediacaran macrobiota: Gondwana Research, v. 27, p. 1355–1380, https://doi.org/10.1016/j.gr.2014.11.002.
Macdonald, F.A., Swanson-Hysell, N.L., Park, Y., Lisiecki, L., and Jagoutz, O., 2019, Arc-continent collisions in the tropics set Earth's climate state: Science, v. 364, p. 181–184, https://doi.org/10.1126/science.aav5300.
Mallmann, G., Chemale, F., Ávila, J.N., Kawashita, K., and Armstrong, R.A., 2007, Isotope geochemistry and geochronology of the Nico Pérez terrane, Rio de la Plata craton, Uruguay: Gondwana Research, v. 12, p. 489–508, https://doi.org/10.1016/j.gr.2007.01.002.
Martin, H., 1965, The Precambrian Geology of South West Africa and Namaqualand: Cape Town, South Africa, University of Cape Town, 4 plates.
Martin, M.W., Grazhdankin, D.V., Bowring, S.A., Evans, D.A.D., Fedonkin, M.A., and Kirschvink, J.L., 2000, Age of Neoproterozoic bilaterian body and trace fossils, White Sea, Russia: Implications for metazoan evolution: Science, v. 288, p. 841–845, https://doi.org/10.1126/science.288.5467.841.
Maslov, A., Meert, J., Levashova, N., Yu, R., Grazhdankin, D., Kuznetsov, N., Krupenin, M., Fedorova, N.M., and Ipat'eva, I.S., 2013, New constraints for the age of Vendian glacial deposits (Central Urals): Doklady Earth Sciences, v. 449, p. 303–308, https://doi.org/10.1134/S1028334X13030203.
Matthews, J.J., 2015, The Stratigraphical Context of the Ediacaran Biota of Eastern Newfoundland: Oxford, UK, University of Oxford, https://ora.ox.ac.uk/objects/uuid:852682cc-aa5a-42b9-83fd-4dd013ebc21b.
Matthews, J.J., Liu, A.G., Yang, C., McIlroy, D., Levell, B., and Condon, D.J., 2021, A chronostratigraphic framework for the rise of the Ediacaran macrobiota: New constraints from Mistaken Point Ecological Reserve, Newfoundland: Geological Society of America Bulletin, v. 133, p. 612–624, https://doi.org/10.1130/B35646.1.
McIlroy, D., and Brasier, M.D., 2017, Ichnological evidence for the Cambrian explosion in the Ediacaran to Cambrian succession of Tanafjord, Finnmark, northern Norway, *in* Brasier, A.T., McIlroy, D., and McLoughlin, N., eds., Earth System Evolution and Early Life: A Celebration of the Work of Martin Brasier: Geological Society, London, Special Publication 448, p. 351–368, https://doi.org/10.1144/SP448.7.
McIlroy, D., et al., 2026, Ediacaran endlings from the Avalon assemblage and the severity of the Kotlin crisis: First documentation of the Inner Meadow Lagerstätte, Newfoundland, Canada: Geology, v. 54, p. 342–347, https://doi.org/10.1130/G54217.1.
McMahon, W.J., Liu, A.G., Tindal, B.H., and Kleinhans, M.G., 2020, Ediacaran life close to land: Coastal and

shoreface habitats of the Ediacaran macrobiota, the Central Flinders Ranges, South Australia: Journal of Sedimentary Research, v. 90, p. 1463–1499, https://doi.org/10.2110/jsr.2020.029.

Meinhold, G., Arslan, A., Jensen, S., and Kühnemann, V., 2025, Discovery of trace fossils in the Weesenstein Group, Elbe zone, Germany, and its significance for revising the Ediacaran and Ordovician stratigraphy of Saxo-Thuringia: Geological Magazine, v. 162, p. e10, https://doi.org/10.1017/S0016756825000032.

Menon, L., 2015, Ediacaran Discoidal Impressions and Related Structures from Newfoundland, Canada, and the Long Mynd, Shropshire, UK: Their Nature and Biogenicity: Oxford, UK, University of Oxford, https://ora.ox.ac.uk/objects/uuid:ff1dc37f-711d-41f2-a3b8-733cd26cb571.

Menon, L.R., McIlroy, D., and Brasier, M.D., 2013, Evidence for Cnidaria-like behavior in ca. 560 Ma Ediacaran *Aspidella*: Geology, v. 41, p. 895–898, https://doi.org/10.1130/G34424.1.

Merdith, A.S., Gernon, T.M., Maffre, P., Donnadieu, Y., Goddéris, Y., Longman, J., Müller, R.D., and Mills, B.J.W., 2025, Phanerozoic icehouse climates as the result of multiple solid-Earth cooling mechanisms: Science Advances, v. 11, https://doi.org/10.1126/sciadv.adm9798.

Miller, N., Johnson, P., and Stern, B., 2008, Marine versus non-marine environments for the Jibalah Group, NW Arabian shield: A sedimentologic and geochemical survey and report of possible metazoa in the Dhaiqa formation: Arabian Journal for Science and Engineering, v. 33, p. 55–77.

Mills, A.J., Dunning, G.R., Murphy, M., and Langille, A., 2017, New geochronological constraints on the timing of magmatism for the Bull Arm Formation, Musgravetown Group, Avalon terrane, northeastern Newfoundland, *in* Current Research 2017: Newfoundland and Labrador Department of Natural Resources Geological Survey Report 17-1, p. 1–17, https://www.gov.nl.ca/iet/files/mines-geoscience-publications-currentresearch-2017-mills-dunning-2017.pdf.

Mills, A.J., Normore, L., Gomez, N., Dunning, G.R., and Lowe, D.G., 2024, A tale of two basins: Juxtaposition of the Ediacaran fossil-bearing St. John's Basin against the Ediacaran glaciovolcanic Bonavista Basin on the Bonavista Peninsula, Avalon zone, Newfoundland: Atlantic Geoscience, v. 60, p. 131–150, https://doi.org/10.4138/atlgeo.2024.007.

Mills, B.J.W., Krause, A.J., Scotese, C.R., Hill, D.J., Shields, G.A., and Lenton, T.M., 2019, Modelling the long-term carbon cycle, atmospheric CO_2, and Earth surface temperature from late Neoproterozoic to present day: Gondwana Research, v. 67, p. 172–186, https://doi.org/10.1016/j.gr.2018.12.001.

Molén, M.O., 2023, Glaciation-induced features or sediment gravity flows—An analytic review: Journal of Palaeogeography, v. 12, p. 487–545, https://doi.org/10.1016/j.jop.2023.08.002.

Moncrieff, A.C.M., 1989, Classification of poorly-sorted sedimentary rocks: Sedimentary Geology, v. 65, p. 191–194, https://doi.org/10.1016/0037-0738(89)90015-8.

Moynihan, D.P., Strauss, J.V., Nelson, L.L., and Padget, C.D., 2019, Upper Windermere Supergroup and the transition from rifting to continent-margin sedimentation, Nadaleen River area, northern Canadian Cordillera: Geological Society of America Bulletin, v. 131, p. 1673–1701, https://doi.org/10.1130/B32039.1.

Muscente, A.D., et al., 2019, Ediacaran biozones identified with network analysis provide evidence for pulsed extinctions of early complex life: Nature Communications, v. 10, 911, https://doi.org/10.1038/s41467-019-08837-3.

Narbonne, G.M., 2005, The Ediacara Biota: Neoproterozoic origin of animals and their ecosystems: Annual Review of Earth and Planetary Sciences, v. 33, p. 421–442, https://doi.org/10.1146/annurev.earth.33.092203.122519.

Narbonne, G.M., and Hofmann, H.J., 1987, Ediacaran biota of the Wernecke Mountains, Yukon, Canada: Palaeontology, v. 30, p. 647–676.

Narbonne, G.M., Laflamme, M., Trusler, P.W., Dalrymple, R.W., and Greentree, C., 2014, Deep-water Ediacaran fossils from northwestern Canada: Taphonomy, ecology, and evolution: Journal of Paleontology, v. 88, p. 207–223, https://doi.org/10.1666/13-053.

Nelson, L.L., Ramezani, J., Almond, J.E., Darroch, S.A.F., Taylor, W.L., Brenner, D.C., Furey, R.P., Turner, M., and Smith, E.F., 2022, Pushing the boundary: A calibrated Ediacaran-Cambrian stratigraphic record from the Nama Group in northwestern Republic of South Africa: Earth and Planetary Science Letters, v. 580, https://doi.org/10.1016/j.epsl.2022.117396.

Niu, Y., Shi, G.R., Zhang, Q., Jones, B.G., Wang, X., and Zhao, G., 2024, Ediacaran Cordilleran-type mountain ice sheets and their erosion effects: Earth-Science Reviews, v. 249, https://doi.org/10.1016/j.earscirev.2023.104671.

Noble, S.R., Condon, D.J., Carney, J.N., Wilby, P.R., Pharaoh, T.C., and Ford, T.D., 2015, U-Pb geochronology and global context of the Charnian Supergroup, UK: Constraints on the age of key Ediacaran fossil assemblages: Geological Society of America Bulletin, v. 127, p. 250–265, https://doi.org/10.1130/B31013.1.

O'Connell, B., McMahon, W.J., Nduutepo, A., Pokolo, P., Mocke, H., McMahon, S., Boddy, C.E., and Liu, A.G., 2025, Transport of 'Nama'-type biota in sediment gravity and combined flows: Implications for terminal Ediacaran palaeoecology: Sedimentology, v. 72, p. 365–407, https://doi.org/10.1111/sed.13239.

Oyhantçabal, P., Siegesmund, S., Wemmer, K., Frei, R., and Layer, P., 2007, Post-collisional transition from calc-alkaline to alkaline magmatism during transcurrent deformation in the southernmost Dom Feliciano belt (Braziliano–Pan-African, Uruguay): Lithos, v. 98, p. 141–159, https://doi.org/10.1016/j.lithos.2007.03.001.

Pagani, M., Huber, M., and Sageman, B., 2014, Greenhouse climates, *in* Holland, H.D., and Turekian, K.K., eds., Treatise on Geochemistry, Volume 6: The Oceans and Marine Geochemistry (2nd edition): Amsterdam, Elsevier, p. 281–304, https://doi.org/10.1016/B978-0-08-095975-7.01314-0.

Palacios, T., 2024, The oldest fossil record in the Iberian Peninsula; lower Ediacaran acritarchs of the Tentudía Formation, Ossa-Morena zone (OMZ), southwest Iberian Massif: Journal of Iberian Geology, v. 50, p. 667–682, https://doi.org/10.1007/s41513-024-00266-6.

Pang, K., Wu, C., Sun, Y., Ouyang, Q., Yuan, X., Shen, B., Lang, X., Wang, R., Chen, Z., and Zhou, C., 2021, New Ediacara-type fossils and late Ediacaran stratigraphy from the northern Qaidam Basin (China): Paleogeographic implications: Geology, v. 49, p. 1160–1164, https://doi.org/10.1130/G48842.1.

Pauley, J.C., 1991, A revision of the stratigraphy of the Longmyndian Supergroup, Welsh Borderland, and of its relationship to the Uriconian Volcanic Complex: Geological Journal, v. 26, p. 167–183, https://doi.org/10.1002/gj.3350260209.

Pazos, P.J., Rapalini, A.E., Bettucci, L.S., and Tófalo, O.R., 2011, The Playa Hermosa Formation, Playa Verde Basin, Uruguay, *in* Arnaud, E., Halverson, G.P., and Shields-Zhou, G., eds., The Geological Record of Neoproterozoic Glaciations: Geological Society, London, Memoir 36, p. 547–553, https://doi.org/10.1144/M36.52.

Pecoits, E., 2003, Sedimentología y consideraciones estratigráficas de la Formación Las Ventanas en su área tipo, departamento de Maldonado, Uruguay, *in* Bossi, J., ed., Estratigrafía del Precámbrico de Uruguay—Terrenos Tectono-Estratigráficos y Geocronología: Revista de la Sociedad Uruguaya de Geologia Publicacion Especial 1, p. 124–140.

Pecoits, E., Gingras, M., Aubet, N., and Konhauser, K., 2008, Ediacaran in Uruguay: Palaeoclimatic and palaeobiological implications: Sedimentology, v. 55, p. 689–719, https://doi.org/10.1111/j.1365-3091.2007.00918.x.

Pecoits, E., Gingras, M.K., and Konhauser, K.O., 2011, Las Ventanas and San Carlos formations, Maldonado Group, Uruguay, *in* Arnaud, E., Halverson, G.P., and Shields-Zhou, G., eds., The Geological Record of Neoproterozoic Glaciations: Geological Society, London, Memoir 36, p. 555–564, https://doi.org/10.1144/M36.53.

Penn, J.L., Deutsch, C., Payne, J.L., and Sperling, E.A., 2018, Temperature-dependent hypoxia explains biogeography and severity of end-Permian marine mass extinction: Science, v. 362, https://doi.org/10.1126/science.aat1327.

Perry, A.L., Low, P.J., Ellis, J.R., and Reynolds, J.D., 2005, Climate change and distribution shifts in marine fishes: Science, v. 308, p. 1912–1915, https://doi.org/10.1126/science.1111322.

Peters, S.E., and Gaines, R.R., 2012, Formation of the 'Great Unconformity' as a trigger for the Cambrian explosion: Nature, v. 484, p. 363–366, https://doi.org/10.1038/nature10969.

Powers, M.C., 1953, A new roundness scale for sedimentary particles: Journal of Sedimentary Research, v. 23, p. 117–119, https://doi.org/10.1306/D4269567-2B26-11D7-8648000102C1865D.

Pu, J.P., Bowring, S.A., Ramezani, J., Myrow, P., Raub, T.D., Landing, E., Mills, A., Hodgin, E., and Macdonald, F.A., 2016, Dodging snowballs: Geochronology of the Gaskiers glaciation and the first appearance of the Ediacaran biota: Geology, v. 44, p. 955–958, https://doi.org/10.1130/G38284.1.

Pyle, L.J., Narbonne, G.M., James, N.P., Dalrymple, R.W., and Kaufman, A.J., 2004, Integrated Ediacaran chronostratigraphy, Wernecke Mountains, northwestern Canada: Precambrian Research, v. 132, p. 1–27, https://doi.org/10.1016/j.precamres.2004.01.004.

Rapalini, A.E., Tohver, E., Bettucci, L.S., Lossada, A.C., Barcelona, H., and Pérez, C., 2015, The late Neoproterozoic Sierra de las Ánimas Magmatic Complex and Playa Hermosa Formation, southern Uruguay, revisited: Paleogeographic implications of new paleomagnetic and precise geochronologic data: Precambrian Research, v. 259, p. 143–155, https://doi.org/10.1016/j.precamres.2014.11.021.

R Core Team, 2021, R: A Language and Environment for Statistical Computing, https://www.R-project.org (accessed January 2025).

Retallack, G.J., 2022, Towards a glacial subdivision of the Ediacaran Period, with an example of the Boston Bay Group, Massachusetts: Australian Journal of Earth Sciences, v. 69, p. 223–250, https://doi.org/10.1080/08120099.2021.1954088.

Rice, A.H.N., Edwards, M.B., Hansen, T.A., Arnaud, E., and Halverson, G.P., 2011, Glaciogenic rocks of the Neoproterozoic Smalfjord and Mortensnes formations, Vestertana Group, E. Finnmark, Norway, *in* Arnaud, E., Halverson, G.P., and Shields-Zhou, G., eds., The Geological Record of Neoproterozoic Glaciations: Geological Society, London, Memoir 36, p. 593–602, https://doi.org/10.1144/M36.57.

Rooney, A.D., Cantine, M.D., Bergmann, K.D., Gómez-Pérez, I., Al Baloushi, B., Boag, T.H., Busch, J.F., Sperling, E.A., and Strauss, J.V., 2020, Calibrating the coevolution of Ediacaran life and environment: Proceedings of the National Academy of Sciences of the United States of America, v. 117, p. 16,824–16,830, https://doi.org/10.1073/pnas.2002918117.

Runnegar, B., Gehling, J.G., Jensen, S., and Saltzman, M.R., 2024, Ediacaran paleobiology and biostratigraphy of the Nama Group, Namibia, with emphasis on the erniettomorphs, tubular and trace fossils, and a new sponge, *Arimasia germsi* n. gen. n. sp.: Journal of Paleontology, v. 98, p. 1–59, https://doi.org/10.1017/jpa.2023.81.

Sánchez Bettucci, L., and Linares, E., 1996, Primeras edades en Basaltos del Complejo Sierra de las Animas, *in* XIII Congreso Geológico Argentino y III Congreso de Exploración de Hidrocarburos, Actas Volumen 1: Buenos Aires, Argentina, Asociación Geológica Argentina, p. 399–404.

Schwellnus, C., 1941, The Nama tillite in the Klein Karas Mountains: Transactions of the Geological Society of South Africa, v. 44, p. 19–33.

Scotese, C.R., Song, H., Mills, B.J.W., and van der Meer, D.G., 2021, Phanerozoic paleotemperatures: The Earth's changing climate during the last 540 million years: Earth-Science Reviews, v. 215, https://doi.org/10.1016/j.earscirev.2021.103503.

Segessenman, D.C., and Peters, S.E., 2024, Transgression-regression cycles drive correlations in Ediacaran–Cambrian rock and fossil records: Paleobiology, v. 50, p. 150–163, https://doi.org/10.1017/pab.2023.31.

Shen, B., Xiao, S., Dong, L., Chuanming, Z., and Liu, J., 2007, Problematic macrofossils from Ediacaran successions in the North China and Chaidam blocks: Implications for their evolutionary roots and biostratigraphic significance: Journal of Paleontology, v. 81, p. 1396–1411, https://doi.org/10.1666/06-016R.1.

Shen, B., Xiao, S., Zhou, C., Kaufman, A.J., and Yuan, X., 2010, Carbon and sulfur isotope chemostratigraphy of the Neoproterozoic Quanji Group of the Chaidam Basin, NW China: Basin stratification in the aftermath of an Ediacaran glaciation postdating the Shuram event?: Precambrian Research, v. 177, p. 241–252, https://doi.org/10.1016/j.precamres.2009.12.006.

Shields, G.A., Mills, B.J.W., Zhu, M., Raub, T.D., Daines, S.J., and Lenton, T.M., 2019, Unique Neoproterozoic carbon isotope excursions sustained by coupled evaporite dissolution and pyrite burial: Nature Geoscience, v. 12, p. 823–827, https://doi.org/10.1038/s41561-019-0434-3.

Socci, A.D., and Smith, G.W., 1990, Stratigraphic implications of facies within the Boston Basin, *in* Socci, A.D., Skehan, J.W., and Smith, G.W., eds., Geology of the Composite Avalon Terrane of Southern New England: Geological Society of America Special Paper 245, p. 55–74, https://doi.org/10.1130/SPE245-p55.

Song, H., Huang, S., Jia, E., Dai, X., Wignall, P.B., and Dunhill, A.M., 2020, Flat latitudinal diversity gradient caused by the Permian–Triassic mass extinction: Proceedings of the National Academy of Sciences of the United States of America, v. 117, p. 17,578–17,583, https://doi.org/10.1073/pnas.1918953117.

Środoń, J., et al., 2023, Ages of the Ediacaran Volyn-Brest trap volcanism, glaciations, paleosols, Podillya Ediacaran soft-bodied organisms, and the Redkino-Kotlin boundary (East European craton) constrained by zircon single grain U-Pb dating: Precambrian Research, v. 386, https://doi.org/10.1016/j.precamres.2023.106962.

Stockey, R.G., Pohl, A., Ridgwell, A., Finnegan, S., and Sperling, E.A., 2021, Decreasing Phanerozoic extinction intensity as a consequence of Earth surface oxygenation and metazoan ecophysiology: Proceedings of the National Academy of Sciences of the United States of America, v. 118, https://doi.org/10.1073/pnas.2101900118.

Summerhayes, C.P., 2020, Palaeoclimatology: From Snowball Earth to the Anthropocene: New York, John Wiley & Sons, 560 p.

Surprenant, R.L., and Droser, M.L., 2024, New insight into the global record of the Ediacaran tubular morphotype: A common solution to early multicellularity: Royal Society Open Science, v. 11, https://doi.org/10.1098/rsos.231313.

Tasistro-Hart, A.R., and Macdonald, F.A., 2023, Phanerozoic flooding of North America and the Great Unconformity: Proceedings of the National Academy of Sciences of the United States of America, v. 120, https://doi.org/10.1073/pnas.2309084120.

Thomas, R.J., et al., 2002, Precambrian evolution of the Sirwa Window, Anti-Atlas orogen, Morocco: Precambrian Research, v. 118, p. 1–57, https://doi.org/10.1016/S0301-9268(02)00075-X.

Thompson, M.D., and Bowring, S.A., 2000, Age of the Squantum "tillite," Boston Basin, Massachusetts: U-Pb zircon constraints on terminal Neoproterozoic glaciation: American Journal of Science, v. 300, p. 630–655, https://doi.org/10.2475/ajs.300.8.630.

Thompson, M.D., Grunow, A.M., and Ramezani, J., 2007, Late Neoproterozoic paleogeography of the southeastern New England Avalon zone: Insights from U-Pb geochronology and paleomagnetism: Geological Society of America Bulletin, v. 119, p. 681–696, https://doi.org/10.1130/B26014.1.

Tindal, B., 2023, Geological Constraints on Neoproterozoic Glacial Episodes [Ph.D. thesis]: Cambridge, UK, University of Cambridge, 275 p., https://doi.org/10.17863/CAM.93553.

Vickers-Rich, P., et al., 2012, Reconnaissance for an Ediacaran Fauna, Kingdom of Saudi Arabia: Saudi Geological Survey Technical Report SGS-TR-2013–5, 21 p.

Waggoner, B., 2003, The Ediacaran biotas in space and time: Integrative and Comparative Biology, v. 43, p. 104–113, https://doi.org/10.1093/icb/43.1.104.

Wang, C., Evans, D.A.D., Li, M., Zhang, J.-H., Han, J., Wen, B., Wang, J., and Zhao, J.-F., 2022, Proterozoic–Mesozoic development of the Quanji block from northern Tibet and the cratonic assembly of eastern Asia: American Journal of Science, v. 322, p. 705–727, https://doi.org/10.2475/05.2022.03.

Wang, R., Shen, B., Lang, X., Wen, B., Mitchell, R.N., Ma, H., Yin, Z., Peng, Y., Liu, Y., and Zhou, C., 2023a, A Great late Ediacaran ice age: National Science Review, v. 10, no. 8, https://doi.org/10.1093/nsr/nwad117.

Wang, R., Yin, Z., and Shen, B., 2023b, A late Ediacaran ice age: The key node in the Earth system evolution: Earth-Science Reviews, v. 247, https://doi.org/10.1016/j.earscirev.2023.104610.

Wang, X., Zhang, X., and Liu, W., 2021a, Biostratigraphic constraints on the age of Neoproterozoic glaciation in North China: Journal of Asian Earth Sciences, v. 219, https://doi.org/10.1016/j.jseaes.2021.104894.

Wang, X.-P., Chen, Z., Pang, K., Zhou, C.-M., Xiao, S., Wan, B., and Yuan, X.-L., 2021b, *Dickinsonia* from the Ediacaran Dengying Formation in the Yangtze Gorges area, South China: Palaeoworld, v. 30, p. 602–609, https://doi.org/10.1016/j.palwor.2021.01.002.

Wang, Z., Wang, J., Suess, E., Wang, G., Chen, C., and Xiao, S., 2017, Silicified glendonites in the Ediacaran Doushantuo Formation (South China) and their potential paleoclimatic implications: Geology, v. 45, p. 115–118, https://doi.org/10.1130/G38613.1.

Wang, Z., Chen, C., Wang, J., Suess, E., Chen, X., Ma, X., Wang, G., and Xiao, S., 2020, Wide but not ubiquitous distribution of glendonite in the Doushantuo Formation, South China: Implications for Ediacaran climate: Precambrian Research, v. 338, https://doi.org/10.1016/j.precamres.2019.105586.

Westerhold, T., et al., 2020, An astronomically dated record of Earth's climate and its predictability over the last 66 million years: Science, v. 369, p. 1383–1387, https://doi.org/10.1126/science.aba6853.

Wickham, H., et al., 2019, Welcome to the Tidyverse: Journal of Open Source Software, v. 4, https://doi.org/10.21105/joss.01686.

Wong Hearing, T.W., Pohl, A., Williams, M., Donnadieu, Y., Harvey, T.H.P., Scotese, C.R., Sepulchre, P., Franc, A., and Vandenbroucke, T.R.A., 2021, Quantitative comparison of geological data and model simulations constrains early Cambrian geography and climate: Nature Communications, v. 12, 3868, https://doi.org/10.1038/s41467-021-24141-5.

Wood, R., Liu, A.G., Bowyer, F., Wilby, P.R., Dunn, F.S., Kenchington, C.G., Cuthill, J.F.H., Mitchell, E.G., and Penny, A., 2019, Integrated records of environmental change and evolution challenge the Cambrian Explosion: Nature Ecology & Evolution, v. 3, p. 528–538, https://doi.org/10.1038/s41559-019-0821-6.

Wood, R., Bowyer, F.T., Alexander, R., Yilales, M., Uahengo, C.-I., Kaputuaza, K., Ndeunyema, J., and Curtis, A., 2023, New Ediacaran biota from the oldest Nama Group, Namibia (Tsaus Mountains), and re-definition of the Nama Assemblage: Geological Magazine, v. 160, p. 1673–1686, https://doi.org/10.1017/S0016756823000638.

Woodhouse, A., Swain, A., Fagan, W.F., Fraass, A.J., and Lowery, C.M., 2023, Late Cenozoic cooling restructured global marine plankton communities: Nature, v. 614, p. 713–718, https://doi.org/10.1038/s41586-023-05694-5.

Wu, C., Hua, H., Zeng, Z., Zheng, Y., Yang, D., and Jiao, R., 2024a, An Ediacaran glacial deposit in southern margin of the North China craton: The Luoquan Formation—Sedimentology, geochronology and provenance: Geological Journal, v. 59, p. 2336–2363, https://doi.org/10.1002/gj.5022.

Wu, C., Pang, K., Chen, Z., Wang, X., Zhou, C., Wan, B., Yuan, X., and Xiao, S., 2024b, The rangeomorph fossil *Charnia* from the Ediacaran Shibantan biota in the Yangtze Gorges area, South China: Journal of Paleontology, v. 98, no. 2, p. 232–248, https://doi.org/10.1017/jpa.2022.97.

Xiao, Q., She, Z., Wang, G., Li, Y., Ouyang, G., Cao, K., Mason, R., and Du, Y., 2020, Terminal Ediacaran carbonate tempestites in the eastern Yangtze Gorges area, South China: Palaeogeography, Palaeoclimatology, Palaeoecology, v. 547, https://doi.org/10.1016/j.palaeo.2020.109681.

Xiao, S., Bao, H., Wang, H., Kaufman, A.J., Zhou, C., Li, G., Yuan, X., and Ling, H., 2004, The Neoproterozoic Quruqtagh Group in eastern Chinese Tianshan: Evidence for a post-Marinoan glaciation: Precambrian Research, v. 130, p. 1–26, https://doi.org/10.1016/j.precamres.2003.10.013.

Xiao, S., Chen, Z., Pang, K., Zhou, C., and Yuan, X., 2021, The Shibantan Lagerstätte: Insights into the Proterozoic-Phanerozoic transition: Journal of the Geological Society, v. 178, https://doi.org/10.1144/jgs2020-135.

Xiao, S.H., and Narbonne, G.M., 2020, The Ediacaran Period, *in* Gradstein, F.M., Ogg, J.G., Schmitz, M.D., and Ogg, G.M., eds., Geologic Time Scale 2020: Amsterdam, Elsevier, p. 521–561, https://doi.org/10.1016/B978-0-12-824360-2.00018-8.

Yang, C., Rooney, A.D., Condon, D.J., Li, X.-H., Grazhdankin, D.V., Bowyer, F.T., Hu, C., Macdonald, F.A., and Zhu, M., 2021, The tempo of Ediacaran evolution: Science Advances, v. 7, https://doi.org/10.1126/sciadv.abi9643.

Yao, J., Xiao, S., Yin, L., Li, G., and Yuan, X., 2005, Basal Cambrian microfossils from the Yurtus and Xishanblaq Formations (Tarim, North-West China): Systematic revision and biostratigraphic correlation of *Micrhystridium*-like acritarchs: Palaeontology, v. 48, p. 687–708, https://doi.org/10.1111/j.1475-4983.2005.00484.x.

Youbi, N., Ernst, R.E., Söderlund, U., Boumehdi, M.A., Lahna, A.A., Tassinari, C.C.G., Moume, W.E., and Bensalah, M.K., 2020, The Central Iapetus magmatic province: An updated review and link with the ca. 580 Ma Gaskiers glaciation, *in* Adatte, T., Bond, D.P.G., and Keller, G., eds., Mass Extinctions, Volcanism, and Impacts: New Developments: Geological Society of America Special Paper 544, p. 35–66, https://doi.org/10.1130/2020.2544(02).

Zhou, C., Li, X.-H., Xiao, S., Lan, Z., Ouyang, Q., Guan, C., and Chen, Z., 2017, A new SIMS zircon U-Pb date from the Ediacaran Doushantuo Formation: Age constraint on the Weng'an biota: Geological Magazine, v. 154, p. 1193–1201, https://doi.org/10.1017/S0016756816001175.

Zhou, C., Yuan, X., Xiao, S., Chen, Z., and Hua, H., 2019, Ediacaran integrative stratigraphy and timescale of China: Science China Earth Sciences, v. 62, p. 7–24, https://doi.org/10.1007/s11430-017-9216-2.

Zieger-Hofmann, M., et al., 2022, Correlation of Neoproterozoic diamictites in southern Namibia: Earth-Science Reviews, v. 233, https://doi.org/10.1016/j.earscirev.2022.104159.

Science Editor: Troy Rasbury
Associate Editor: Daniel Peppe

Manuscript Received 26 November 2025
Revised Manuscript Received 13 March 2026
Manuscript Accepted 14 July 2026